Terms and Conditions of Use of Digitised Theses from Trinity College Library Dublin

Copyright statement

All material supplied by Trinity College Library is protected by copyright (under the Copyright and Related Rights Act, 2000 as amended) and other relevant Intellectual Property Rights. By accessing and using a Digitised Thesis from Trinity College Library you acknowledge that all Intellectual Property Rights in any Works supplied are the sole and exclusive property of the copyright and/or other IPR holder. Specific copyright holders may not be explicitly identified. Use of materials from other sources within a thesis should not be construed as a claim over them.

A non-exclusive, non-transferable licence is hereby granted to those using or reproducing, in whole or in part, the material for valid purposes, providing the copyright owners are acknowledged using the normal conventions. Where specific permission to use material is required, this is identified and such permission must be sought from the copyright holder or agency cited.

Liability statement

By using a Digitised Thesis, I accept that Trinity College Dublin bears no legal responsibility for the accuracy, legality or comprehensiveness of materials contained within the thesis, and that Trinity College Dublin accepts no liability for indirect, consequential, or incidental, damages or losses arising from use of the thesis for whatever reason. Information located in a thesis may be subject to specific use constraints, details of which may not be explicitly described. It is the responsibility of potential and actual users to be aware of such constraints and to abide by them. By making use of material from a digitised thesis, you accept these copyright and disclaimer provisions. Where it is brought to the attention of Trinity College Library that there may be a breach of copyright or other restraint, it is the policy to withdraw or take down access to a thesis while the issue is being resolved.

Access Agreement

By using a Digitised Thesis from Trinity College Library you are bound by the following Terms & Conditions. Please read them carefully.

I have read and I understand the following statement: All material supplied via a Digitised Thesis from Trinity College Library is protected by copyright and other intellectual property rights, and duplication or sale of all or part of any of a thesis is not permitted, except that material may be duplicated by you for your research use or for educational purposes in electronic or print form providing the copyright owners are acknowledged using the normal conventions. You must obtain permission for any other use. Electronic or print copies may not be offered, whether for sale or otherwise to anyone. This copy has been supplied on the understanding that it is copyright material and that no quotation from the thesis may be published without proper acknowledgement.

Simulated annealing of Skyrme model configurations

by

Shane Magee

B.A. (Mod.)

A Thesis submitted to
The University of Dublin
for the degree of

Phd

Department of Mathematics
University of Dublin
Trinity College

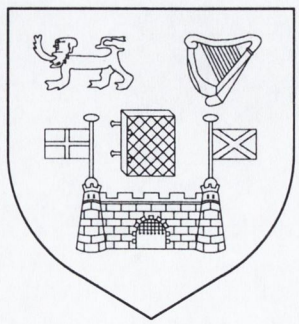

October, 2005

Declaration

I declare that:

1. This has not previously been submitted as an exercise for a degree at this or any other university.

2. This work is my own except where noted in the text.

3. The library should lend or copy this work upon request.

4. Portions of this work have appeared in the following papers:

   - C.J. Houghton and S. Magee, *A zero mode quantization of the Skyrmion*, Phys. Lett. **B632** (2006) 593
   - C.J. Houghton and S. Magee, *Pion mass effects on Skyrme configurations*, submitted to Phys. Lett. **B**.

Shane Magee

Shane Magee (October 31st 2005)

Summary

The Skyrme model is a topological field theory that has been shown to be a good low-energy approximation to QCD. A particular quantum theoretical treatment of the model reduces the quantization to a finite-dimensional quantum mechanical problem, selecting significant degrees of freedom of the configuration and quantizing them. A long-asked question has been how the quantized configuration differs from the classical minimum.

Simulated annealing is a well-known technique for finding global minima of energy functions in configuration spaces with numerous local minima. We use it here to find the Skyrme model configuration that minimizes the energy obtained when the quantized spin and isospin modes are included. We include these modes without any prior assumptions of symmetry.

We find that the quantized isorotational energy is an average of energies obtained from rotations around all symmetry axes, and that it has only a radially expanding effect on the minimum configuration.

We also find that the chiral symmetry breaking term corresponding to the inclusion of a pion mass has a substantial effect on higher charge configurations. We find, for the examples we have studied so far, the configuration becomes more elongated for large pion masses provided the polyhedral skeleton around which the zero pion mass baryon density is distributed is non-Platonic.

There are no limits to our capacities
Because we have the infinite Divine
Within us.

Sri Chinmoy

Acknowledgements

I would like to thank my supervisor, Conor Houghton, for being a model of patience, kindness and good humour during these past four years.
Most of the computational work was performed on the IITAC and Moloch high performance clusters belonging to the Trinity Centre for High Performance Computing. I'd like to thank Dermot Frost, Robert Crosbie and Jimmy Tang for taking the time mid-apocalypse to start me on my way. I also used the Walton cluster at the Irish Centre for High-End computing; I'd like to thank Gemma Kinsella and Niall Moran for helping me to get started there. I would like to thank the Higher Education Authority for their PRTLI grant, and Trinity College for the start-up grant and Postgraduate Award.
I would like to thank my office-mates Justin, Alan, and especially Richie for being angelically quiet whilst we were all writing up. On the sanity-maintenance front, I'd like to thank Ambarish, Mangala, Colm, Paula, Gary and Vinny. Thanks to Jesper Olsen for a very timely dose of inspiration.

To my parents,

who have only ever wanted to see their children happy.

Contents

Chapter 1

Introduction

The experimental confirmation by Rutherford [1] of the absence of electrons in the nucleus gave rise to the realization that there was an internucleonic force that overcame the electrostatic force between protons and kept the nucleus together. The development of Quantum Chromodynamics (QCD) in the late 1960's and early 1970's gave us a description of this 'strong' force at a fundamental level within the nucleon itself. The long-term goal of nuclear physics is the derivation of physical observables from QCD. QCD is non-perturbative at low energies, and the main approach in this area is using lattice QCD simulations. However, at the present time most lattice QCD simulations work with lattices not much larger than the size of a single nucleon, and it is not expected that lattice QCD simulations will be able to obtain direct predictions with the precision of existing data in the near future. Nuclear physics does have well-developed phenomenological models based on separated nucleons interacting via potentials constrained by nucleon-nucleon scattering data, but there is no underlying theory determining the setting of the many parameters needed to fit the model accurately to data, and the search for a connection with QCD is in its infancy. As yet, there is no quantitative understanding of the strong interaction at the level at which it was first discovered.

One possibility is to use an effective theory that is a good approximation to QCD at nuclear energies. At low energies, QCD approximates a mesonic theory with pion fields as the dominant fields in the limit of the number of colours (N_c) going to infinity

[2, 3]. There are only three quark colours in SU(3) QCD, of course, but it is felt that this approach is a promising starting point for describing low energy phenomenology, such as the dynamics of light nuclei. No-one knows what this large-N_c effective theory should look like, except that it should produce solitonic baryon solutions and that to a first approximation the phenomenological behaviour should be similar to a theory of pion fields only. The simplest reasonable choice for such a theory is the Skyrme model.

The Skyrme model is a classical field theory originally developed [4] as part of the original search for a description of the strong interaction. The theory treats baryons as solitonic configurations of pion fields, identifying the baryon number B with the soliton's winding number. A very good review of early work in the the Skyrme model and large-N_c QCD can be found in [5].

Notwithstanding its connection to low-energy QCD, the Skyrme model is an interesting model to study in its own right. The theory has proved capable of describing at least some aspects of nuclear behaviour. The main features of the nucleon-nucleon interaction can be deduced from the model, including the short range repulsion corresponding to the Pauli exclusion principle [6]. For light nuclei, Skyrme configurations are most stable when considering baryon numbers corresponding to ^{4}He and ^{7}Li, the stable nuclei in that region [7]. Of particular importance is the simple quantization of the Skyrmion of unit baryon number [8], which gives reasonable predictions of nucleon and delta resonance properties.

The Skyrme model is also remarkable in that soliton configurations corresponding to baryons can be obtained from a mesonic field. Bound-state Skyrme configurations exist for values of B greater than one [9] and the minimum energy configurations have a skeletal structure with a very high degree of symmetry [10], as illustrated by the examples in figure 1. In most minimum energy configurations, the baryon density is concentrated around a spherical shell away from the origin. The $B = 2$ solution is shaped like a torus, and the configurations have Platonic symmetries in the cases of $B = 3$ (tetrahedron), $B = 4$ (cube) and $B = 7$ (dodecahedron). Almost all of the minimum energy Skyrme configurations found so far have a skeletal structure

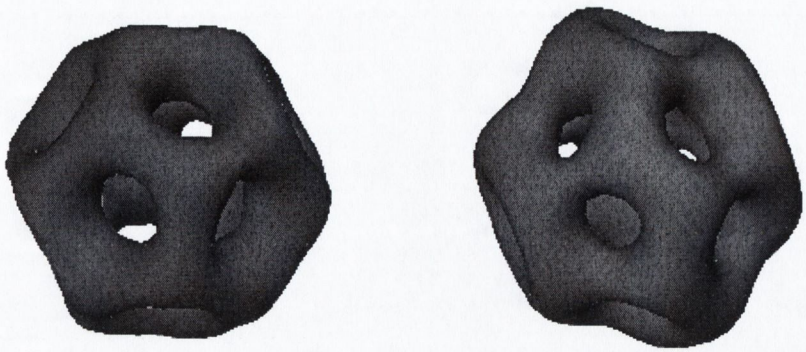

Figure 1-1: Baryon density isosurfaces of classical Skyrme configurations of baryon number seven and eight. The baryon density of the $B = 7$ configuration is distributed around a dodecahedral skeleton; for the $B = 8$ the skeleton is fullerene-shaped.

consisting of three-way vertices characteristic of fullerenes; a Skyrme configuration has even been found that resembles a buckyball.

The Skyrme model is non-renormalizable, and no serious attempts have been made at a full quantum field theoretical treatment. Most quantization approaches have reduced the Skyrme model to a finite-dimensional quantum mechanical system, quantizing the relevant particle degrees of freedom. For a static Skyrme solution, the relevant degrees of freedom are the spin and isospin rotational modes and the vibrational modes. The energy of a classical Skyrme configuration does not change under spatial rotation or rotation in isospin space; therefore, the spin and isospin degrees of freedom are called the *zero modes* of the solution. Pioneering work in Skyrme model quantization was done [8] in which the zero modes of the classical $B = 1$ minimum energy solution were quantized. Subsequent quantization approaches [12, 13] allowed the shape of the $B = 1$ Skyrme configuration to move away from the classical minimum under rotations, and showed that Skyrme configurations require a sufficiently high pion mass m_π to be stable.

However, so far these changes in the configuration were made while still maintaining spherical or axial symmetry. The true zero mode quantized configurations are those that minimize the total energy obtained by quantizing the rotational and isorotational degrees of freedom without any symmetry assumptions. Such configurations might be the key to addressing one current unanswered question in the

Skyrme model; namely, that the ground state quantum numbers obtained for some Skyrme configurations do not match those of their counterparts in nature [14, 15]. The allowed quantum numbers depend on the topology of the space of zero modes, which in turn depend on the symmetries of the configuration; perhaps allowing the rotational and isorotational degrees of freedom to change the configuration shape will give quantum numbers consistent with experiment.

The effect of adding a term to the Skyrme energy corresponding to the addition of a pion mass is itself a topic of current interest. With the addition of this term, the baryon charge density of the minimum energy solution is spread more evenly throughout the configuration volume, and so a minimum energy configuration with pion mass has a shorter mean radius than a minimum energy configuration of the same baryon number with zero pion mass. As we have discussed, when the configuration has zero mass much of the baryon density is concentrated on the surface, and so the size of the configuration scales as $\sqrt[2]{B}$. However, due to the volume contribution of the pion mass, the size of nuclei scale as $\sqrt[3]{B}$, in agreement with experiment. There are also indications [16] that the pion mass causes significant changes to the structure of minimum energy Skyrme configurations. The shell like structures that are the minimum in the massless case might no longer be the minimum if a large enough pion mass is added, and it is an open question what the new configurations might be, or even if for some values of B there is any bound configuration at all.

Put simply, our goal in this research is to find out what effect the zero modes and the pion mass have on Skyrme configurations. To do this, we require a means where given a Skyrme energy functional, the configuration corresponding to the minimum energy of the functional can be obtained in such a way that the structure of the configuration is clearly visible. However, the space of all possible Skyrme configurations is dotted with local energy minima whose number increases as more degrees of freedom are considered, and a minimization algorithm that goes straight for the nearest minimum may well end up trapped in a configuration that is not a global minimum. A perturbative method which is able to move out of local minima is needed.

The simulated annealing algorithm is such a method; it also has the advantages

of being robust and easy to apply to a wide range of problems. In addition, advances in computing speed mean we can now compute minimum energy configurations in a reasonable time, using general formulae for the energy of a rotating Skyrme configuration that do not make any prior assumptions about symmetry. A definitive zero-mode quantization is now within reach.

In the next chapter, we shall give a more detailed account of the Skyrme model, including the topological and quantization issues of interest to us, before expanding in detail upon our own approach. The third chapter contains a description of our implementation of the simulated annealing algorithm, and describes the features peculiar to perturbing a topological configuration on a discretized lattice. An adaptation of the algorithm whereby 3D configurations can be annealed on 2D lattices using axial symmetry is described. In the fourth chapter we shall present the results of our simulations. We investigate the effects of high pion masses on Skyrme configurations, first focusing on the $B = 8$ case, which has low binding energy and a ground state with no zero mode energy. We then investigate other values of B, and produce a general hypothesis about the effect of pion masses on minimum energy solutions. We produce new results for the Skyrme configurations modelling the nucleon and delta, and determine the effect of the rotational energy on higher charge Skyrme configurations. The last chapter will be given to concluding remarks and some ideas about how to proceed onwards from our work.

Chapter 2

The Skyrme model

2.1 Introduction

The Skyrme model is a non-linear sigma model, im which the dynamics are described by a scalar meson field $\sigma(x)$ and a pseudoscalar pion field $\boldsymbol{\pi}$, with the constraint $\sigma^2 + \boldsymbol{\pi}.\boldsymbol{\pi} = F_\pi^2/4$, where F_π is a constant.

These fields can be incorporated into an SU(2)) matrix U:

$$U = \frac{2}{F_\pi}\left(\sigma\,\mathbf{1}_2 + i\boldsymbol{\pi}..\boldsymbol{\tau}\right), \tag{2.1}$$

where $\mathbf{1}_2$ is the 2×2 identity matrix and $\boldsymbol{\tau}$ are tthe Pauli matrices. U can be seen as the expansion around the vacuum expectation value $\boldsymbol{\pi} = 0$ of the exponentiation

$$U = \exp\left(\frac{2i}{F_\pi}\boldsymbol{\pi}.\boldsymbol{\tau}\right). \tag{2.2}$$

Written in terms of the vector currents $R_\mu = \partial_\mu U U^\dagger$ of the field $U(\mathbf{x})$, the Skyrme model has the Lagrangian

$$\begin{aligned} L \;=\; \int \mathrm{d}^3\mathbf{x}\, \Bigg[& \frac{-F_\pi^2}{16}\mathrm{Tr}\left(R_\mu R^\mu\right) + \frac{1}{32e^2}\mathrm{Tr}\left([R_\mu, R_\nu][R^\mu, R^\nu]\right) \\ & + \frac{1}{8}m_\pi^2 F_\pi^2\ \mathrm{Tr}\left(U-1\right)\Bigg], \end{aligned} \tag{2.3}$$

where m_π and e, along with F_π, are free parameters of the model.

The classical Skyrme mass for a static field $U_s(\mathbf{x})$ can be derived from this Lagrangian and is

$$E_{cl} = E_2 + E_4 + E_m \tag{2.4}$$

where

$$\begin{aligned} E_2 &= -\frac{F_\pi^2}{16}\int \mathrm{d}^3\mathbf{x}\ \mathrm{Tr}\left(R_i R_i\right) \\ E_4 &= -\frac{1}{32e^2}\int \mathrm{d}^3\mathbf{x}\ \frac{1}{32e^2}\left([R_i, R_j][R_i, R_j]\right) \\ E_m &= -\frac{1}{8}m_\pi^2 F_\pi^2 \int \mathrm{d}^3\mathbf{x}\ \mathrm{Tr}\left(U-1\right). \end{aligned} \tag{2.5}$$

2.1.1 The sigma model term

E_2 is the unique term that is second order in the derivatives of the σ and $\boldsymbol{\pi}$ fields:

$$E_2 = \frac{1}{2}\left[(\partial_\mu \sigma)^2 + (\partial_\mu \boldsymbol{\pi})^2\right] \tag{2.6}$$

and is generally referred to as the sigma model term. Solitonic configurations with baryon number exist as solutions of the sigma model term on its own. However, these configurations are not energetically stable in 3D space by Derrick's theorem [17]. This can be seen by a rescaling of $U(\mathbf{x})$ as $\mathbf{x}$ goes to $\lambda\mathbf{x}$. The integration measure $\mathrm{d}^3\lambda\mathbf{x}$ transforms as

$$\mathrm{d}^3(\lambda\mathbf{x}) \rightarrow \left(\lambda^3 \mathrm{d}^3\mathbf{x}\right) \tag{2.7}$$

and the spatial derivative $\partial\,\partial(\lambda x_i)$ as

$$\frac{\partial}{\partial(\lambda x_i)} \rightarrow \left(\frac{1}{\lambda}\right)\frac{\partial}{\partial x_i} \tag{2.8}$$

Therefore, the scaled energy E_2^λ is

$$E_2^\lambda \rightarrow \frac{1}{\lambda}E_2 \tag{2.9}$$

Clearly, energetically favourable configurations have zero energy, and the resulting Skyrmion collapses to a point.

2.1.2 The Skyrme term

The E_4 term was added by Skyrme to stabilize the soliton, and is commonly referred to as the Skyrme term. In this case, the energy scales as $E_4^\lambda \to \lambda E_4$. We can easily verify that with the addition of the Skyrme term a true minimum is obtained, and Skyrmion collapse is prevented:

$$\begin{aligned} \frac{\partial E(\lambda \mathbf{x})}{\partial \lambda} = 0 \quad &\Rightarrow \quad \frac{E_2}{E_4} = 1 \\ \frac{\partial^2 E(\lambda \mathbf{x})}{\partial \lambda^2} = 0 \quad &\Rightarrow \quad E_2 > 0 \end{aligned}$$

There are other possible four-derivative integrands we could place in the Lagrangian which could stabilize the soliton, for example $\mathrm{Tr}\left[(\partial R_\mu)^2\right]$, but the Skyrme term is the unique term that gives rise to a positive Hamiltonian and also the unique term that gives rise to a Hamiltonian that is second order in time derivatives. The latter is especially important because there are problems with the stability of the classical solution once terms of higher order in time derivatives are included.

Stable 3D configurations can also be produced by adding higher-order energies to the sigma model term, for example a sixth-order term E_6 [19]. However, the addition of such terms as higher-order corrections to the Skyrme mass (2.4) seem to have no effect on the structure of the minimum energy configuration, save for a slight radial expansion [20, 21].

2.1.3 The pion mass term

The third term in the energy, E_m, is a chiral symmetry breaking term first added in [18]. Inserting the pion expansion (2.2) of U into the E_m, we see that it is indeed a

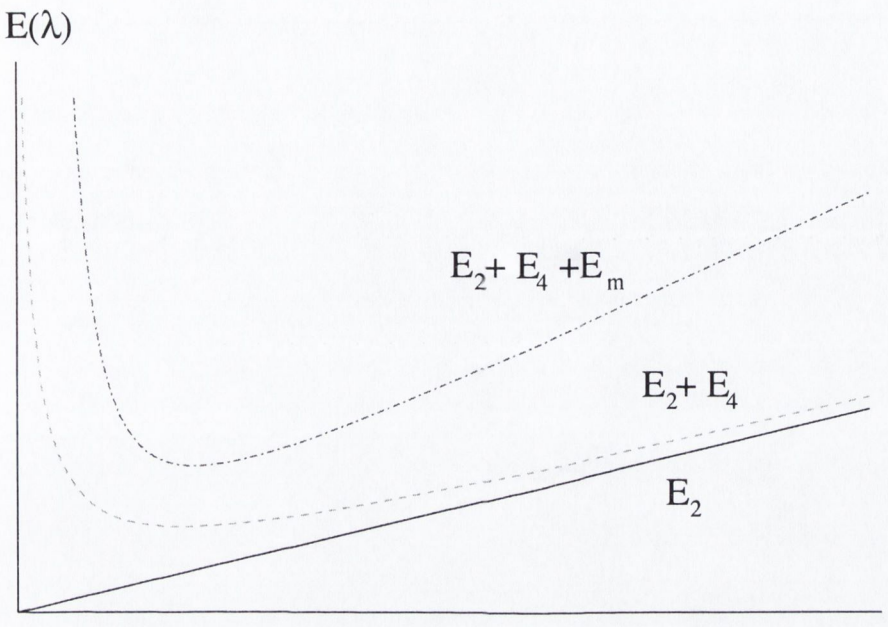

Figure 2-1: Plot showing how the energy changes as the length scales from $\mathbf{x} \rightarrow \lambda\mathbf{x}$. The solid line shows the sigma model term only, the dashed line is with the Skyrme term added and the dotted line is with both Skyrme and sigma model terms added.

mass potential term, with m_π as the pion mass:

$$E_m = \frac{1}{2} m_\pi^2 \int \mathrm{d}^3\mathbf{x} \ (\boldsymbol{\pi}.\boldsymbol{\pi}) \tag{2.10}$$

The pion mass term scales as

$$E_m^\lambda \rightarrow \frac{1}{\lambda^3} E_m \tag{2.11}$$

Both the sigma model and Skyrme terms are invariant under the SU(2) $\times$ SU(2) chiral transformation sending $U \rightarrow GUH^{-1}$, where G and H are arbitrary SU(2) matrices. In nature, SU(2) $\times$ SU(2) chiral symmetry is only good to within 5%-10%, and it was argued that a symmetry breaking term might yield a closer fit to nature in their quantization approach than that obtained in [8]. Introducing this term did not modify the minimum energy solution significantly for the nucleon and delta resonance cases studied in [18]; however, the term has been retained in many Skyrme model approaches to counteract instabilities in the quantized configuration caused by rotation. These instabilities will be discussed in section 2.4.

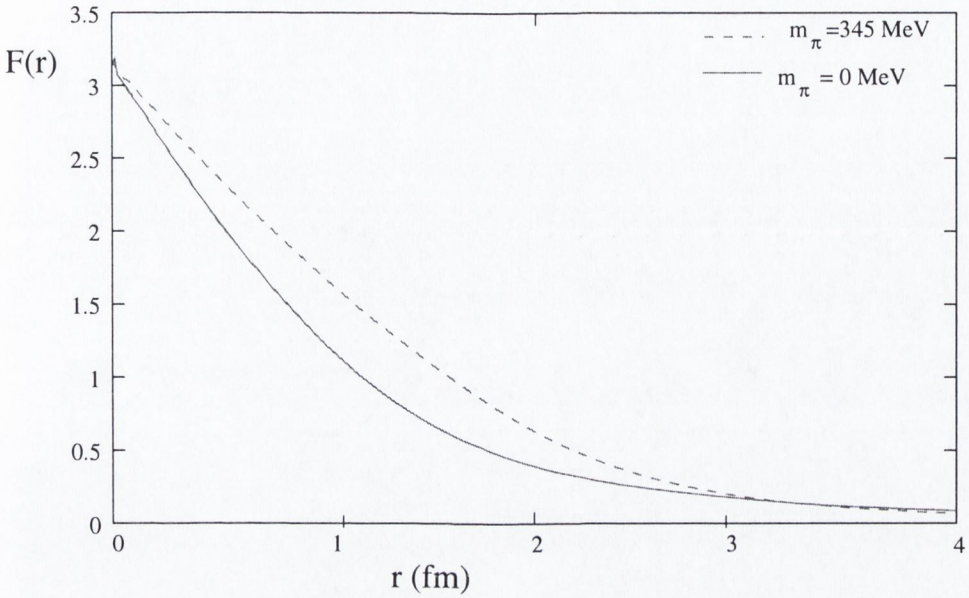

Figure 2-2: Plot of the numerically determined profile function for the minimum energy $B = 1$ configuration in the hedgehog ansatz as a function of radius r from the origin, for pion mass values of $m_\pi = 0$ and $m_\pi = 345$ MeV.

2.1.4 Energy and length scales

We can scale the parameters F_π and e out of the sigma model and Skyrme terms entirely by setting appropriate energy and length scales: a choice of $F_\pi/4e$ as our unit of energy and $2/eF_\pi$ as our unit of length yields

$$L = \int \mathrm{d}^3\mathbf{x} \; -\frac{1}{2}\,\mathrm{Tr}\,(R_\mu R^\mu) + \frac{1}{16}\,\mathrm{Tr}\,([R_\mu, R_\nu][R^\mu, R^\nu]) + m^2\,\mathrm{Tr}\,(U-1) \qquad (2.12)$$

where for convenience we use the scaled pion mass $m = 2m_\pi/F_\pi$. The scaling changes the static Skyrme energy functional to

$$E = \int \mathrm{d}^3\mathbf{x} \left[-\frac{1}{2}\,\mathrm{Tr}\,(R_i R_i) - \frac{1}{16}\,([R_i, R_j][R_i, R_j]) - m^2\,\mathrm{Tr}\,(U-1) \right]. \qquad (2.13)$$

2.1.5 The hedgehog ansatz

An important solution to the Euler-Lagrange equation of the Skyrme model is the unit baryon number 'hedgehog' ansatz suggested by Skyrme

$$U = \mathrm{e}^{if(r)\mathbf{n}.\boldsymbol{\tau}}. \qquad (2.14)$$

The hedgehog moniker derives from the fact the the pion field vectors all point radially outward.

A radial function $f(r)$ that takes a value of π at the origin and tends to zero at long distances yields a Skyrme configuration with unit baryon number. Indeed, $f(r)$ can be numerically generated such that the hedgehog map describes the minimum energy $B = 1$ Skyrme configuration. Numerical solutions for zero and nonzero pion mass are shown in figure 2-2.

2.1.6 A note on symmetry

We described the elegant symmetries of Skyrme configurations in the introduction; we need to say a little more about what we mean by symmetry. For example, we do not mean by spherical symmetry that the Skyrme field is just a function of the radius r; such configurations have no winding number. When we refer to the spatial symmetry of the solution, we mean that a symmetry transformation acting on the Skyrme configuration in space can be compensated by a transformation in isospin space of the form

$$U \to AUA^{\dagger} \tag{2.15}$$

where $A \in \mathrm{SU}(2)$. This isospin symmetry comes from the spontaneous breaking of the chiral symmetry brought about by the constraint that the field tend to the vacuum at long distances. The simplest way of distinguishing the two rotations is to say that the spatial rotation rotates the coordinates $\mathbf{x}$, whereas rotations in isospin space, known as isorotations, rotate the pion fields $\boldsymbol{\pi}$. Defining a spatial field symmetry this way makes the physically observable energy and baryon charge densities $\mathcal{E}$ and $\mathcal{B}$ strictly invariant under that symmetry.

2.2 Sigma model topology

The Skyrme field $U(\mathbf{x})$ is a mapping from $\mathbb{R}^3 \rightarrow \mathrm{SU}(2)$, and hence to its group manifold S^3. However, in order to keep the configuration energy finite we must impose a suitable long-distance constraint. The condition

$$\lim_{|\mathbf{x}|\rightarrow\infty} U(\mathbf{x}) = 1 \tag{2.16}$$

maps all points at infinity in $\mathbb{R}^3$ to one point, compactifying the domain $\mathbb{R}^3$ to the topological three-dimensional sphere S^3. As detailed below, the map $S^3 \rightarrow S^3$ is non-trivial; it is possible to split the set of all such maps into distinct subsets that are not continuously deformable into each other. These subsets are known as homotopy or Chern-Pontryagin classes.

More technically, the homotopy classes of a map from the n-sphere S^n to any topological space X form a group known as the n-th homotopy group of X and denoted $\pi_n(X)$. Thus, the homotopy group of our mapping is $\pi_n(S^3)$. For all $k, \pi_k\left(S^k\right)$ is isomorphic to $\mathbb{Z}$ [22], and we shall refer to the integer label of $\pi_n(S^3)$ as the topological charge or winding number. The important point is that, since any time evolution of the configuration can be understood as a homotopy transformation, the corresponding winding numbers are conserved independently of the dynamics.

To construct an explicit form for the winding number of a configuration in the space $\mathcal{Q}$ of all Skyrme configurations

$$B : \mathcal{Q} \rightarrow \mathbb{Z} \tag{2.17}$$

in the Skyrme model, we must first write down the normalized volume element in the range SU(2):

$$\Omega = \frac{1}{24\pi^2}\mathrm{Tr}\left(\mathrm{d}UU^{-1} \wedge \mathrm{d}UU^{-1} \wedge \mathrm{d}UU^{-1}\right) \tag{2.18}$$

The degree of the Skyrme map $U : S^3 \rightarrow SU(2)$ is independent of Ω and given by the pull-back of Ω to the domain S^3:

$$\begin{aligned}\deg U &= -\frac{1}{24\pi^2}\int \mathrm{d}^3\mathbf{x}\ \mathrm{Tr}\left(\partial_1 U U^{-1}\mathrm{d}x_1 \wedge \partial_2 U U^{-1}\mathrm{d}x_2 \wedge \partial_3 U U^{-1}\mathrm{d}x_3\right) \\ &= -\frac{\epsilon^{ijk}}{24\pi^2}\int \mathrm{d}^3\mathbf{x}\ \mathrm{Tr}\left(R_i R_j R_k\right) \end{aligned} \tag{2.19}$$

The integrand is the Jacobian $J(\mathbf{x})$ of the map at $\mathbf{x}$.

We shall now show that deg U takes integer values, and is, thus, the winding number B of the map U [23]. We choose an element $\hat{U}$ of SU(2) such that the set of points $\{\mathbf{x}_1, ..., \mathbf{x}_m\}$ in $\mathbb{R}_3$ that get mapped to $\hat{U}$ have non-zero Jacobians for the map. The function

$$B = \sum_{k=1}^{m} \mathrm{sign}\ (J(x_k)) \tag{2.20}$$

counts the points x_k, adding -1 if the orientation of $\hat{U}$ is reversed at x_k. B is clearly an integer; we now show that $B = \deg U$ and is thus independent of the choice of $\hat{U}$.

If the volume element Ω is deformed to a small neighbourhood of $\hat{U}$, then its pull-back $U^*(\Omega)$ is concentrated around the points $\{\mathbf{x}_1, ..., \mathbf{x}_m\}$. The integral of $U^*(\Omega)$ over a neighbourhood of a point x_i

$$\int_{B(x_i)} \mathrm{d}^3\mathbf{x}\ J(\mathbf{x}) \tag{2.21}$$

is ± 1 depending on the orientation of U: we demonstrate this by a naïve change of coordinates from x to $\hat{U}$

$$\int_{B(x_i)} \mathrm{d}^3\mathbf{x}\ \frac{J(\mathbf{x})}{|J(\mathbf{x})|}\Omega \tag{2.22}$$

which is equal to the sign of $J(\mathbf{x})$. Summing over all x_i reproduces the formula (2.20).

This winding number was equated to the baryon number by Skyrme [4]; a more physical justification in terms of large-N_c QCD [24] shows that the integrand is in fact equal to the conserved Noether current associated to the baryon charge. The baryon number provides a lower bound on the minimum mass of a Skyrme configuration. Rewriting the Skyrme energy (2.13) using the skew-hermeticity of R_i, and applying

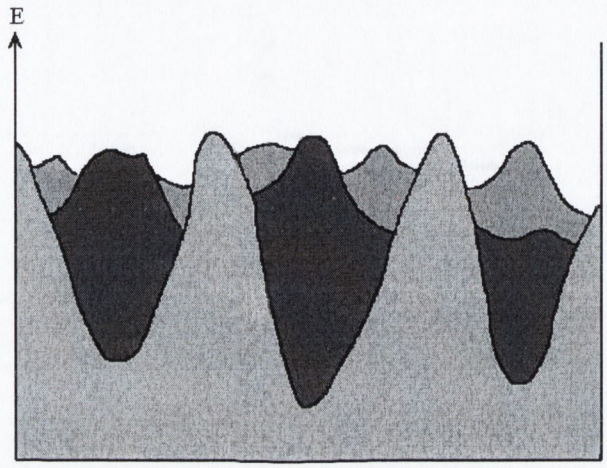

Figure 2-3: The likely shape of Skyrme configuration space for $B > 1$; many local minima with energies quite close to each other. In Chapter 3 we shall conclude that simulated annealing is the best approach to finding a minimum energy solution in such a landscape.

the Cauchy-Schwarz inequality, we obtain

$$\begin{aligned} E &= -\frac{1}{2}\int \mathrm{d}^3\mathbf{x}\ \mathrm{Tr}\left[(R_i)^2 + \frac{1}{2}\left(\epsilon^{ijk}R_jR_k\right)^2\right] \\ &\geq -\frac{1}{2}\int \mathrm{d}^3\mathbf{x}\ |\epsilon^{ijk}\,\mathrm{Tr}\,(R_iR_jR_k)\,|, \end{aligned} \tag{2.23}$$

or

$$E \geq 12\pi^2|B|. \tag{2.24}$$

Equation (2.24) is sometimes referred to as the Bogomol'ny bound; in fact no non-trivial Skyrme configuration exists such that this bound is completely saturated.

2.2.1 Solutions with $B > 1$

As described in the introduction, minimum energy Skyrme configurations with baryon number greater than unity have a high degree of symetry. Two or more bound state solutions with different symmetries exist for each value of $B > 1$, and the number of solutions with different symmetry tend to increase with B.

Identifying minimum energy solutions has not always been a straightforward process; for several values of B, minimum energy configurations were incorrectly identified which turned out to have different symmetries than the actual minimum energy configurations. In some cases, the energy minima for two different structures corresponding to the same value of B have been so close as to be almost degenerate; examples of this are $B = 10, 13$ and 16. Almost all values of $B > 10$ have solutions with different symmetry than the minimum energy solution but not much higher energy. For $B < 10$, very little research has been done into higher energy solutions, but the same is probably true to a lesser extent. Due to the structure change, the energy barrier between bound states of the same charge B is probably quite high. Thus we can conclude that the energy 'landscape' mapped out by the space $\mathcal{Q}$ of Skyrme configurations most likely consists of many local minima with deep potential wells. In addition, the number of local minima in the the configuration space of baryon number B solutions $\mathcal{Q}(B)$ increases with B.

2.3 The rational map ansatz

Many shell-like solutions of higher minimum energy solutions of baryon number $B > 1$ are similar in appearance to BPS monopole solutions of the same monopole number. The rational map ansatz was developed in [25] as a means of easily approximating minimum energy solutions; it was motivated by a similar association of rational maps to monopoles [26].

A rational map is a function from $S^2 \rightarrow S^2$ which is holomorphic in the Riemann sphere coordinates $z = \tan(\theta/2)\, e^{i\phi}$. A general rational map of degree B has, as the name suggests, the form

$$R(z) = \frac{q_1 z^B + q_2 z^{B-1} + ... q_{B-1} z + q_B}{p_1 z^B + p_2 z^{B-1} + ... p_{B-1} z + p_B}. \tag{2.25}$$

In the ansatz, the unit vector which appears in the Skyrme hedgehog 2.14 ansatz,

$$\mathbf{n} = (\sin\theta\cos\phi, \sin\theta\sin\phi, \cos\theta) \tag{2.26}$$

$$= \left(\frac{\mathrm{Re} z}{1+|z|^2}, \frac{\mathrm{Im} z}{1+|z|^2}, \frac{1-|z|^2}{1+|z|^2} \right), \tag{2.27}$$

is replaced by a unit vector written in terms of rational maps

$$\mathbf{n}_R = \left(\frac{\mathrm{Re} R(z)}{1+|R(z)|^2}, \frac{\mathrm{Im} R(z)}{1+|R(z)|^2}, \frac{1-|R(z)|^2}{1+|R(z)|^2} \right), \tag{2.28}$$

giving rise to a new field ansatz:

$$U = e^{-if(r)\mathbf{n}_R \cdot \boldsymbol{\sigma}}. \tag{2.29}$$

Any function $f(r)$ which has $f(0) = \pi$ and tends asymptotically to zero for large r will yield a map with baryon number B. To find approximations to the minimum energy solution, $R(z)$ is first simplified using the symmetries of the known charge-B minimum energy solution. Numerical algorithms are then used to find profile functions $f(r)$ that minimize the rational map energy, E_{rat}, obtained by inserting

the ansatz into the classical energy (2.13):

$$E_{rat} = 4\pi \int_0^\infty \mathrm{d}r \left\{ r^2 \left(\frac{\partial f}{\partial r}\right)^2 + 2B \left[\left(\frac{\partial f}{\partial r}\right)^2 + 1 \right] \sin^2 f + \mathcal{I} \frac{\sin^4 f}{r^2} + 2m^2 (1 - \cos f) \right\} \tag{2.30}$$

where

$$\mathcal{I} = \frac{1}{4\pi} \int \left(\frac{1 + |z|^2}{1 + |R|^2} \left| \frac{dR}{dz} \right| \right)^4 \frac{2i\, dz\, d\bar{z}}{(1 + |z|^2)^2} \tag{2.31}$$

is a real-valued function that depends only on $R(z)$. Rational maps that minimize $\mathcal{I}$ have been numerically computed for all $B \leq 40$; the integrand is independent of m_π and so the rational map (2.25) that mimimizes $\mathcal{I}$ is the same for solutions with and without pion mass. Using the minimized value of $\mathcal{I}$, profile functions that minimize the rational map energy (2.30) can be obtained by one-dimensional simulated annealing.

Originally the map was used to model solutions with $m_\pi = 0$, and produced energies only a few percent above those of the numerically determined minima. It is not known if ansätze modelling configurations with high pion masses are as accurate as those modelling configurations with zero pion mass, simply because minimum energy configurations with large pion mass are not yet available. By obtaining these minimum energy configurations using simulated annealing, we will then be able to compare them to their rational map counterparts.

2.4 Skyrme model quantization

A seminal paper on Skyrme model quantization is that of Adkins et al. [8], in which the $B = 1$ Skyrme 'hedgehog' ansatz (2.14) is quantized. The calculation obtaining the zero mode Lagrangian of a general Skyrme configuration is described in section 2.5; in the specific case of the hedgehog ansatz, the Lagrangian becomes

$$L = -E_{cl} + \frac{1}{2}\Lambda\omega^2 \tag{2.32}$$

where ω is the angular velocity of the rotation; for spherically symmetric configurations spatial rotations and rotations in isospin space are equivalent. E_{cl} is the classical energy (2.13) written in terms of the hedgehog ansatz profile function $f(r)$:

$$E_{cl} = 4\pi \int_0^\infty \mathrm{d}r \left\{ r^2 \left(\frac{\partial f}{\partial r}\right)^2 + 2\left[\left(\frac{\partial f}{\partial r}\right)^2 + 1\right]\sin^2 f + \frac{\sin^4 f}{r^2} \right\}, \tag{2.33}$$

and Λ is the moment of inertia:

$$\Lambda = 4\pi \int_0^\infty \mathrm{d}r\, r^2 \sin^2 f \left[1 + \left(\frac{\partial f}{\partial r}\right)^2 + \frac{\sin^2 f}{r^2}\right]. \tag{2.34}$$

Introducing the conjugate angular momentum $J = \Lambda\omega$, and defining quantum states on which the operator J^2 has the eigenvalue $\hbar^2 j(j+1)$, we write down the quantum Hamiltonian

$$H = E_{cl} + \frac{J^2}{2\Lambda} \tag{2.35}$$

This approach is often referred to as 'rigid-body' quantization, as the inertia of the classical Skyrme configuration is used to calculate the quantized rotational energy; in this approach, quantization does not change the minimum energy configuration. But the softness of the soliton with respect to shape changes away from the hedgehog ansatz configuration was soon recognized [27, 28], and it was clear that the most obvious zero-mode correction to the rigid-body result was to allow for the possibility of the shape of the Skyrme configuration changing as a result of spin and isospin rotations. This can be done in a straightforward manner, by allowing the Skyrme

configuration to minimize the full Hamiltonian (2.35) instead of just E_{cl}; the resulting Euler-Lagrange equation can be solved numerically, and was done so in [12] with the addition of the pion mass energy term. For convenience, we shall just show the leading terms in the Euler-Lagrange equation to order $1/r^2$:

$$\frac{\partial^2 f}{\partial r^2} + \frac{2}{r}\frac{\partial f}{\partial r} + \frac{j\,(j+1)}{4\Lambda^2}\sin 2f - m_\pi^2 \sin f = 0 \tag{2.36}$$

Thus the function $f\,(r)$ has a Yukawa-like decay as $r \to \infty$:

$$f\,(r) \sim \frac{1}{r}\exp\left(-\sqrt{m_\pi^2 - \frac{j\,(j+1)}{2\Lambda^2}}\,r\right) \tag{2.37}$$

The pion mass m_π, therefore, sets an upper limit as to how fast the configuration can rotate. Beyond this limit $f\,(r)$ is oscillatory, and the configuration has infinite energy. The experimental value of $m_\pi = 138 MeV$ is too small to enable the Skyrmion to spin fast enough to match nucleon and delta resonance masses without becoming unstable. A new calculation [29] showed that proper fits of F_π and e to experimental data can be obtained only by increasing m_π to well above its experimental value.

2.4.1 Effect of quantization on Skyrme parameters

The quantities F_π and e have usually been treated as the free parameters of the Skyrme model. Those working on the model have largely tended to adopt the values of $e = 4.84$ and $F_\pi = 108$ MeV obtained as a result of rigid-body Skyrme quantization with m_π set to its experimental value of 138 MeV [18]. These values were found by comparing quantized nucleon and delta resonance masses to experiment. Although there are no values of F_π and e that would produce stable Skyrme models of either the nucleon or the delta resonance with the experimental pion mass, the parameters obtained in [18] have remained in use as a means of comparing different approaches to the Skyrme model. As described above, one can fit $B = 1$ data to the Skyrme model for large values of the pion mass, and future approaches may use parameters similar to the set of $m_\pi = 345$ MeV, $e = 4.84$ and $F_\pi = 108$ MeV obtained in [29].

On the other hand, Skyrme parameters have been obtained up to now using a quantization procedure that only takes into account the zero modes of the configuration. There is evidence that the addition of field and vibrational modes would have a substantial effect on the configuration. The minimum energy solutions of baryon number B are much more tightly bound than their counterparts in nature; for example, a $B = 2$ toroidal configuration has a binding energy of 186 MeV compared to 2 MeV for the deuteron it models [9]. The addition of vibrations to the space of modes to be quantized would reduce this binding energy considerably. A number of investigations of the vibrational modes of various Skyrme configurations have already taken place [30, 31, 32] and some ideas about how to use simulated annealing to incorporate vibrational modes of freedom are given in Chapter 5. Quantum field modes are much more difficult to treat, although a numerical scheme to evaluate the zero point quantum corrections to soliton masses has been examined [33].

A more thorough quantization of the zero mode states might also yield better parameters. Specifically, allowing the configuration to change shape without predetermined symmetries might lower the masses enough to enable stable-configuration fits of F_π and e while constraining m_π to its experimental value. A generalization of rigid-body quantization that will allow us to quantize a Skyrme configuration of any symmetry is described in section 2.5.

2.4.2 Symmetry and higher-charge quantization

A quantization of the Skyrme model yields energy eigenstates with spin l and isospin k. In this section, we shall see that for a given value of baryon number B, there are only certain combinations of l and k which are consistent with quantizing the configuration as a fermion in the case of odd-B configurations, or as a boson in the case of even-B configurations.

Ideally, Skyrme wavefunctions should obey the requirement that we can quantize them as fermions or bosons according to their spin quantum number. Suppose we have a state consisting of one or more separated $B = 1$ Skyrme configurations. If this state is to be quantized as a fermion, the wavefunction $|\psi\rangle$ must change sign

if one of the configurations rotates by 2π. Rotations by 2π are closed paths in Skyrme configuration space $\mathcal{Q}$ that are not continuously deformable to a point; other examples of such closed paths are rotations of a configuration by any angle θ such that $U(\theta) = U(0)$.

These closed paths fall into two homotopy classes [34]; those rotations that are continuously contractible to a point and those that are not. By allocating the following phase to the wavefunction

$$C_{FR} = \begin{cases} 1, & \text{loop is contractible,} \\ -1, & \text{loop is non} - \text{contractible,} \end{cases} \tag{2.38}$$

so that a 2π rotation R has the effect

$$R|\psi\rangle = C_{FR}|\psi\rangle, \tag{2.39}$$

the state can be quantized in two ways, one corresponding to quantizing it as a fermion, the other to quantizing it as a boson. C_{FR} are known as Finkelstein-Rubinstein (FR) constraints. Rotations by 2π of $B = 1$ configurations with half-integer spin are noncontractible [35], and so $B = 1$ configurations corresponding to the nucleon and delta resonance can be quantized as fermions. This result was extended to configurations of all baryon numbers by the observation [24] that 2π rotations are noncontractible if the baryon number is odd, which is the case for half-integer spin.

If a Skyrme configuration is symmetric, there are additional closed paths we can use to constrain l and k. For example, if a configuration has C_2 rotational symmetry about a given axis, then a rotation by π about that axis is a closed path, since $U(\pi) = U(0)$. If a spatial rotation by α followed by an isorotation β is a closed loop, we can apply the FR constraints once we have determined whether the loop is contractible or not. The allowed spin and isospin quantum numbers l and k are then deduced by:

$$e^{-\alpha \mathbf{J}} e^{-i\beta \mathbf{K}} |\psi\rangle = C_{FR}|\psi\rangle. \tag{2.40}$$

The difficulty lies in deciding whether a closed loop is contractible. Rational map ansätze which have the same symmetry as the minimum solution were used to derive a general formula in [14]. Another method [15] relied primarily on separating the configuration into smaller configurations with known contraction properties to obtain the quantum numbers. The results of the two approaches are summarized in table 2.1 for baryon numbers from five to nine. Results for all baryon numbers from 1 to 22 were obtained in [14]. In both approaches the general result is the same: the even-B quantum number match the corresponding experimental value, whereas almost all the odd-B quantum numbers do not.

Both approaches assume that the the ground state quantum numbers are the numbers with the lowest values of l and k consistent with the FR constraints; the underlying assumption being that the dominant terms in the rotational energy have the form

$$E_{rot} = \hbar^2 \left[\frac{l\,(l+1)}{2U} + \frac{k\,(k+1)}{2V} \right], \tag{2.41}$$

where U and V are rotational and isorotational moments of inertia. A change of Hamiltonian might yield a lowest energy state for higher quantum numbers; for example, the addition of a strong spin-isospin cross term, or the generalisation of the Hamiltonian to include spin and isospin inertia tensors with large non-diagonal elements.

However, for some baryon numbers the ground state quantum numbers found in nature are not even allowed by the FR constraints. For example, in the $B = 7$ case the spin $3/2$, isospin $1/2$ state is forbidden, even though those are the quantum numbers of the ground state for the Li^7 isotope. States corresponding to the experimentally determined ground states are in the enlarged set of allowed wavefunctions obtained by combining vibrational modes with the rotational modes [15]; however, some of these states clearly have higher energy than the predicted minimum quantum numbers.

Another possibility is that with the addition of rotational energy, the minimum energy configuration differs from the classical minimum structure so that the FR constraints obtained above are no longer applicable; we should instead find the con-

B	Theory		Expt.		State in rotational spectrum?	State in vibrational spectrum?
	l	k	l	k		
4	0	0	0	0		
5	$\frac{1}{2}$	$\frac{1}{2}$	$\frac{3}{2}$	$\frac{1}{2}$	Not in [15], first excited spin state in [14]	Yes, but $l = \frac{1}{2}, k = \frac{1}{2}$ is lower energy
6	1	0	1	0		
7	$\frac{7}{2}$	$\frac{7}{2}$	$\frac{3}{2}$	$\frac{1}{2}$	No	Yes, but cannot determine if it is ground state
8	0	0	0	0		
9	$\frac{1}{2}$	$\frac{1}{2}$	$\frac{3}{2}$	$\frac{1}{2}$	Not in [15], first excited spin state in [14]	Yes, but $l = \frac{1}{2}, k = \frac{1}{2}$ is lower energy

Table 2.1: The ground state quantum numbers obtained in [15, 14] for B from four to nine are compared with experiment. The second last column asks whether the experimental ground state is in the spectrum of quantum numbers obtained by considering the rotational and isorotational modes. The second column asks whether the ground state numbers are obtained if the rotational modes are combined with vibrational modes as in [15].

figuration that minimizes

$$E = E_{cl} + E_{rot}, \tag{2.42}$$

where E_{cl} is the classical energy functional (2.13) and E_{rot} is obtained without any symmetry assumptions; we shall describe how to do this in the next section. The symmetries of this configuration can then be used to find new FR constraints and hence new quantum numbers l and k which can be compared with experiment.

One indication that this approach might work is given by the fact that the zero mode quantized configuration is more likely be different in shape from the classical minimum in the odd-B sector. The spin and isospin inertias are equal for $B = 1$, but then U increases as B^2 whilst V increases as B, at least when $m_\pi = 0$. Thus, isospin energies are larger than rotational energies, but they do not contribute for the even baryon number states calculated in [15, 14] since k =0. However, k =1/2 for odd-B states, and zero mode energies for odd-B states have more influence on the final configuration than for even-B states.

Another indication is that Skyrme configurations are soft with respect to non rigid-body rotation around an axis, and these rotations tend to reduce the symmetries of the minimum energy configuration. Each symmetry places additional constraints on the wavefunction, and so we expect the spectrum of allowed states to be greater for configurations for which the symmetry has been lowered by rotation.

The approach for obtaining FR constraints for rational maps [14] has been generalised so that constraints can now be obtained from numerically generated configurations [37]. The possibility of finding configurations that yield values of l and k consistent with experiment has been a major motivation in our research.

2.5 A definitive zero mode quantization

Before we derive the general symmetry-independent form of the quantized rotational energy E_{rot}, we should first emphasize the difference between our approach and the rigid-body quantization carried out in [8]; there, the quantization is carried out on the rotational and isorotational modes of an already-determined classical minimum configuration. Rather than investigating the modes of a specific Skyrme configuration, we want to consider the zero-mode space of fields generated from a general static configuration $U_s(\mathbf{x})$ by isorotation C and rotation D:

$$U(\mathbf{x}) = CU_s(D_{ij}x_j)C^\dagger \tag{2.43}$$

where C is in SU(2) form, and D_{ij} is an SO(3) rotational matrix representation of the SU(2) matrix D. All Skyrme configurations obtainable from the classical minimum energy configuration as a result of rotation and isorotation lie within this configuration space. Rotation and isorotation are symmetries of the original Lagrangian (2.12), so classically these configurations are all energy-degenerate.

The effective Lagrangian on this restricted space of configurations can be calculated by treating C and D as time-dependent coordinates. We follow the approach first generalized in [36], inserting the time-dependent field (2.43) into the Lagrangian (2.12) to obtain $L = -E + L_{rot}$, where E is the Skyrmion mass (2.13), and

$$L_{rot} = \int \mathrm{d}^3\tilde{\mathbf{x}} \left(-\frac{1}{2}\mathrm{Tr}\,(F+G)^2 - \frac{1}{8}\mathrm{Tr}\,([R_i, F+G][R_i, F+G]) \right), \tag{2.44}$$

the skew-Hermitian currents F and G are given by

$$\begin{aligned} F &= C^\dagger\dot{C} - UC^\dagger\dot{C}U^\dagger, \\ G &= \dot{D}_{ij}D^{-1}_{jk}\tilde{x}_k R_i, \end{aligned} \tag{2.45}$$

with

$$U = U(\tilde{\mathbf{x}}), \tag{2.46}$$

and

$$\tilde{x}_j = D_{ij} x_i. \tag{2.47}$$

Setting $\Omega_i = -i\mathrm{Tr}\ \sigma_i C^\dagger \dot{C}$, we write $F = \Omega_k T_k$, where

$$T_k = \frac{i}{2}[\sigma_k, U]U^\dagger \tag{2.48}$$

Similarly, setting $\omega_j = -i\mathrm{Tr}\ \sigma_j \dot{B} B^\dagger$ we obtain

$$G = \omega_k \epsilon_{kij} \tilde{x}_i R_j. \tag{2.49}$$

Thus the Lagrangian due to the zero modes is

$$L_{rot} = \frac{1}{2}\omega_i U_{ij} \omega_j + \frac{1}{2}\Omega_i V_{ij} \Omega_j - \omega_i W_{ij} \Omega_j, \tag{2.50}$$

where the matrices U_{ij}, V_{ij} and W_{ij} are given by the following integrals:

$$\begin{aligned}
V_{ij} &= -\int \mathrm{d}^3\mathbf{x} \left[\mathrm{Tr}\,(T_i T_j) + \frac{1}{4}\,\mathrm{Tr}\,([R_k, T_i][R_k, T_j]) \right], \\
W_{ij} &= \epsilon_{jlm} \int \mathrm{d}^3\mathbf{x}\, x_l \left[\mathrm{Tr}\,(T_i R_m) + \frac{1}{4}\,\mathrm{Tr}\,([R_k, T_i][R_k, R_m]) \right], \\
U_{ij} &= -\epsilon_{ilm}\epsilon_{jpq} \int \mathrm{d}^3\mathbf{x}\, x_l x_p \left[\mathrm{Tr}\,(R_m R_q) + \frac{1}{4}\,\mathrm{Tr}\,([R_k, R_m][R_k, R_q]) \right].
\end{aligned} \tag{2.51}$$

L_{rot} can be written as

$$L_{rot} = \frac{1}{2}\tilde{a}_i^\dagger \mathcal{U}_{ij} \tilde{a}_j, \tag{2.52}$$

where

$$\mathcal{U} = \begin{pmatrix} U_{ij} & -W_{ij} \\ -W_{ij} & V_{ij} \end{pmatrix}, \tilde{\mathbf{a}} = \begin{pmatrix} \boldsymbol{\omega} \\ \boldsymbol{\Omega} \end{pmatrix}. \tag{2.53}$$

We define an angular momentum $\tilde{\mathbf{L}}$ canonically conjugate to $\tilde{\mathbf{a}}$:

$$\begin{aligned}\tilde{L}_i &= \frac{\partial L_{rot}}{\partial \tilde{a}_i} \\ &= \frac{1}{2}\left(\mathcal{U}_{ij}\tilde{a}_j + \tilde{a}_j\mathcal{U}_{ji}\right) \\ &= \tilde{a}_j\left(\tilde{\mathcal{U}}\right)_{ji}, \end{aligned} \tag{2.54}$$

where $\tilde{\mathcal{U}}$ is the symmetrization $\frac{1}{2}\left(\mathcal{U}+\mathcal{U}^\dagger\right)$ of $\mathcal{U}$. Thus, the Hamiltonian of the spin and isospin degrees of freedom is

$$H = \frac{1}{2}\tilde{L}_i^\dagger \tilde{\mathcal{U}}_{ij}^{-1}\tilde{L}_j. \tag{2.55}$$

To obtain the eigenvalues of this Hamiltonian we first note that $\tilde{\mathbf{L}}$ can be split up into its spin, $\mathbf{L}$, and isospin, $\mathbf{K}$, parts

$$\tilde{\mathbf{L}} = \begin{pmatrix} \mathbf{L} \\ \mathbf{K} \end{pmatrix} \tag{2.56}$$

For a spin-l, isospin-k particle the angular momentum operators $\mathbf{L}$ can be written as $(2l+1)\times(2k+1)$-dimensional matrix representation $\Sigma_1^L, \Sigma_2^L, \Sigma_3^L$ of SU(2), as can the isospin operators $\Sigma_1^K, \Sigma_2^K, \Sigma_3^K$ of $\mathbf{K}$ for an isospin-n particle. If we define our quantum state as a $|l, l_3\rangle \otimes |k, k_3\rangle$ state, l, l_3 and k, k_3 being the quantum numbers for $\mathbf{L}$ and $\mathbf{K}$ respectively, we can then embed $\mathbf{L}$ and $\mathbf{K}$ into the resulting $\mathrm{SO}(3)^L \times \mathrm{SO}(3)^K$ direct product space:

$$\mathbf{L} \mapsto \hbar\,\boldsymbol{\Sigma}^L \otimes \mathbf{1}_{2k+1} \tag{2.57}$$

$$\mathbf{K} \mapsto \mathbf{1}_{2l+1} \otimes \hbar\,\boldsymbol{\Sigma}^K \tag{2.58}$$

When these representations of $\mathbf{L}$ and $\mathbf{K}$ are inserted into the Hamiltonian H, it becomes a matrix with $(2l+1)\times(2k+1)$ eigenvalues. To calculate the zero mode

Isospin	Spin	Particles applied to
0	$1, 2, 3$	Even-B Nuclei
$\frac{1}{2}$	$\frac{1}{2}, \frac{3}{2}, \frac{5}{2}, \frac{7}{2}$	Odd-B Nuclei
$\frac{3}{2}$	$\frac{3}{2}$	Δ-resonance

Table 2.2: Summary of the zero mode Hamiltonians constructed for use in our simulations

energy E_{rot}, we used an algorithm that calculated all the eigenvalues of H and returned the lowest one. The ground state quantum numbers of the configuration were thus evaluated as the simulated annealing run progressed and allowed, if necessary, to change from the initial quantum numbers.

The quantum numbers l and k should have integer values for even B and half-integer values for odd B. Given this criterion, we then construct Hamiltonians corresponding to those values l and k that are of interest for light nuclei. In all our constructed Hamiltonians, k is kept to its lowest allowed value. This is consistent with nature in the range of B we explore; for nuclei with $B \leq 30$ the number of protons and neutrons are equal for even B, with one necessarily extra neutron for odd B. For $B \geq 30$ there are more neutrons than protons due to electromagnetic effects. It has been pointed out in [15], that if the the zero mode energy is of the form (2.41) in which separate spin and isospin contributions are dominant, then states with high values of k are more likely to be energetically unfavourable than states with high values of l.

Experimental considerations also guide our choice of l; for $B \leq 30$ the nuclear spin reaches a maximum of three. However, we have constructed Hamiltonians for half-integer values of spin up to 7/2; the $l = 7/2, k = 1/2$ Hamiltonian is constructed in response to the corresponding ground state predictions in [15, 14] for $B = 7$. Simulations of the $B = 7$ configuration with the $l = 7/2, k = 1/2$ Hamiltonian can then be compared with simulations using the $l = 3/2, k = 1/2$ Hamiltonian to see which has the lower energy.

Chapter 3

The Simulated Annealing Algorithm

Simulated annealing [38] is a probabilistic searching algorithm used to locate the global minimum of a given function. The algorithm takes its name and inspiration from the annealing process in metallurgy, in which a metal or glass is heated to the point where all the internal stresses and defects within the material have eased, and then cooled slowly. The heat causes the atoms to become unstuck from their initial positions, and the slow cooling allows them to settle in configurations with less energy than the initial energy.

Before the introduction of simulated annealing, or SA for short, algorithm development had focused on the fastest way to navigate the downward slope in the energy 'landscape' towards a minimum. In a landscape with potentially many local minima, this may lead to the configuration being trapped in a minimum that may not actually be the global minimum, a situation analogous to the molecules of a metal being frozen in random positions by sudden quenching. In contrast, SA will temporarily change the system state to states that have higher energy than the initial state. The probability that the algorithm will accept higher energy states is then slowly decreased with time, so that the entire space of possible solutions can be searched for the global minimum.

How do we know SA is the right choice of algorithm for the Skyrme model?

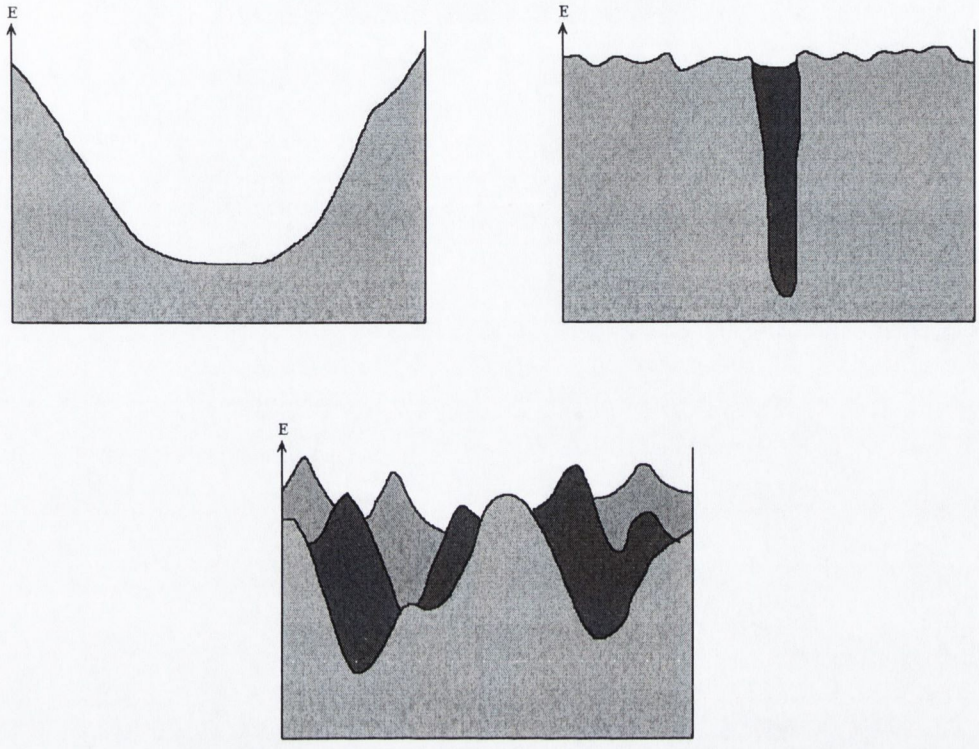

Figure 3-1: Three different energy landscapes: a convex landscape (top left), a 'golf-hole' landscape (top right), and a rugged landscape with many minima ideal for SA (bottom).

There are other algorithms which outperform SA for certain types of configuration space. The most obvious example is the superior performance of the steepest descent method in a purely convex space; but in the Skyrme model we know there are many distinct local minima. Another example perhaps more pertinent to us is the superior performance of a random search algorithm in the 'golf-hole' landscape shown in figure 3-1, characterised by a hollow whose width is negligible compared to the total space. However, the success of conventional calculus-based minimization techniques with small baryon number configurations suggest that the energy hollows are relatively wide. SA seems to be ideally suited for the Skyrme configuration space.

The effective use of SA requires an intuitive knowledge of the energy landscape of configuration space and, as such, its application to specific problems can be considered almost as much of an art as a science. However, simulated annealing on a 3D lattice

has been used before in finding Skyrme solutions. The first approach [43] was a basic feasibility study for values of baryon number B up to four. Recently the technique has been used to evaluate corrections to the minimum energy classical solution caused by the addition of higher order terms [21] to the energy. In our implementation, we build on the suggestions contained in these papers and make considerable improvements of our own.

In order to implement the simulated annealing algorithm, Skyrme configurations are placed on a 3D lattice by assigning the four independent field components of U to each lattice point. For convenience we shall refer to these components as U_μ, defined in terms of the fields σ and $\boldsymbol{\pi}$ as:

$$\begin{aligned} U_0 &= \tfrac{2}{F_\pi}\sigma, \\ U_i &= \tfrac{2}{F_\pi}\pi_i. \end{aligned} \tag{3.1}$$

These components are perturbed in such a way as to preserve the unitarity of U, and the resulting energy change ΔE is computed. The new components are then accepted or rejected according to the Metropolis probability

$$P = \begin{cases} 1 & \Delta E < 0, \\ e^{\frac{-\Delta E}{T}} & \Delta E > 0, \end{cases} \tag{3.2}$$

where T is a temperature parameter that is lowered to zero during the course of the minimization. The algorithm will thus accept large increases in energy near the beginning of the run, freeing the configuration from local energy minima. As T is decreased the algorithm is less likely to accept energy-increasing perturbations, and more likely to reach the bottom of the current energy hollow it finds itself in.

There are two stages to our annealing algorithm, analogous to the heating and cooling stages of a metal:

- An equilibriation stage in which T is mantained at a starting temperature T_{max} until all points on the lattice are thermalized and the system is in equilibrium.

- A cooling stage in which the temperature T is brought from T_{max} to T slowly

enough for the configuration to explore the parameter space and settle on the global minimum.

In an SA simulation, first an initial field configuration is assigned to the lattice. The lattice is then swept through in such a way that field components at every point are perturbed. For each perturbed component or group of components, we accepted or rejected the perturbation based on the probabilities in (3.2). Care has to be taken with perturbing the points; unwanted correlations can arise if neighbouring lattice points are repeatedly perturbed in sequence. We avoided this by storing the accepted points in a backup array and only updating the field points when the entire lattice was perturbed.

This lattice is swept repeatedly, first at $T = T_{max}$ for the equilibriation stage, then with T slowly brought down to zero for the cooling stage. As T goes to zero, the algorithm behaves more and more like a steepest descent algorithm. The algorithm terminates when the field configuration fails to change appreciably over a defined number of lattice iterations.

3.0.1 Generating a starting configuration

In section 2.2, we saw that the Skyrme configuration space is partitioned into disjoint subsets labelled by baryon number B: a simple way of generating configurations for any value of B is required, and it would be additionally useful if the method also could generate good approximations to minimum energy classical solutions for comparison. Furthermore, for higher charge solutions with high pion masses we would like to use smaller lattices; hence a starting configuration that also reproduced the baryon number on smaller lattices would be desirable. For these reasons, the rational map ansatz was usually our initial configuration of choice. To check that the algorithm gave consistent results regardless of the initial configuration used, we also generated initial configurations consisting of separated hedgehog ansätze.

A sequence of SA runs with different starting configurations provided an excellent check on the robustness of the algorithm. The runs that failed to end up at the global minimum gave us intuition for the energy configuration space, which we could use to

readjust the parameters for a nother sequence of runs. This technique was particularly important for studies of rotating configurations to test if certain configurations we obtained were indeed the minimum energy configuration. Our studies in this regard focused on $B = 1$ configurations; there are many interesting profile functions that have already been developed, including functions based on kinks [44] and instantons [46]. We were particularly interested in generating non-spherically symmetric initial configurations to determine whether the final configuration was the same as those generated from spherically symmetric initial conditions.

An increasingly common technique in SA, especially for complicated configuration spaces, is to do many runs with different initial conditions with fast cooling and choose the lowest energy rather than one long run with a slow schedule. The Skyrme configuration space is not so complicated as to warrant this technique for the examples we studied, but it might be an option for higher values of B.

3.0.2 Lattice perturbation

As lattice correlations are already avoided by updating the lattice after all points are swept, the lattice can be swept sequentially. However, we can check whether any bugs have crept into the algorithm by noting the total energy and inertia change as the lattice is swept and comparing it to the energy and inertia obtained by summing over all the local lattice values. In order to do this effectively, it is better to divide the lattice into subgrids of non-neighbouring points and sweep through each subgrid in turn. This can be done without any loss of computational efficiency.

In order to reach the global minimum, it may be necessary for the algorithm to move the Skyrme fields considerably from their initial starting point. However, perturbing the lattice one point at a time is an unacceptably slow means to this end; if the initial starting configuration is very different to the minimum energy configuration, then a perturbation of a single field towards the minimum perturbation is likely to be rejected as the surrounding fields are still in the old configuration.

On the other hand, a cubic block of lattice points perturbed towards the minimum is more likely to be accepted because the energy increase per lattice point is smaller

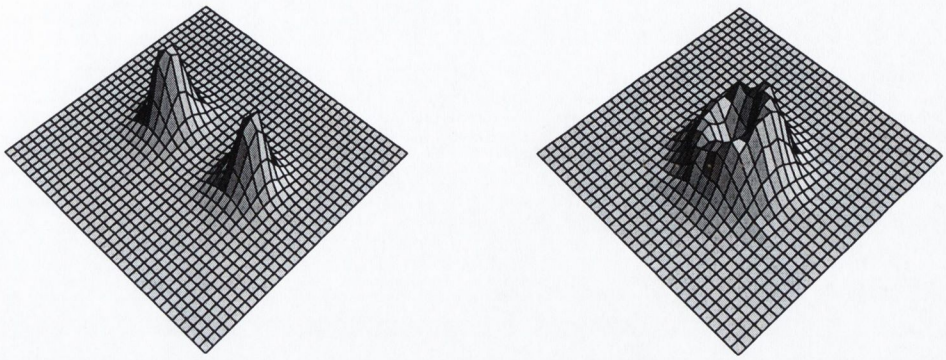

Figure 3-2: Cross-sections of configurations at the points in the graphs shown in figure 3-3 marked "separated nucleons" and "toroidal configuration".

[43]. Upon perturbation the entire plaquette of lattice points is accepted or rejected according to the probability in (3.2). In the equilibriation stage, large plaquettes enable better collective motion of the Skyrme fields, while single perturbations are better for very low T when the configuration structure has been established and the main priority is thermal noise elimination. For this reason, the size of the plaquette is chosen with a T-dependent probability at the beginning of each lattice iteration.

3.0.3 Equilibriation criteria

Typically, when T is kept at T_{max} long enough for the lattice to be fully thermalized, the configuration should have approximately the structure of the minimum energy configuration, albeit with considerable thermal fluctuations. The cooling run will then fine tune the length scale of the configuration and remove the unwanted noise. The important question here is when to stop the equilibriation process and start cooling.

The ideal method of determining if the lattice has fully thermalized is to store the Skyrme field after n, say, lattice iterations; after another n lattice iterations the field is then compared with the previous stored field to see if the configuration has changed. More specifically, if the lattice has equilibriated, a subtraction of the current fields from the stored fields should leave only uncorrelated fluctuations.

However, our implementation, with 26 stored variables associated with each lattice

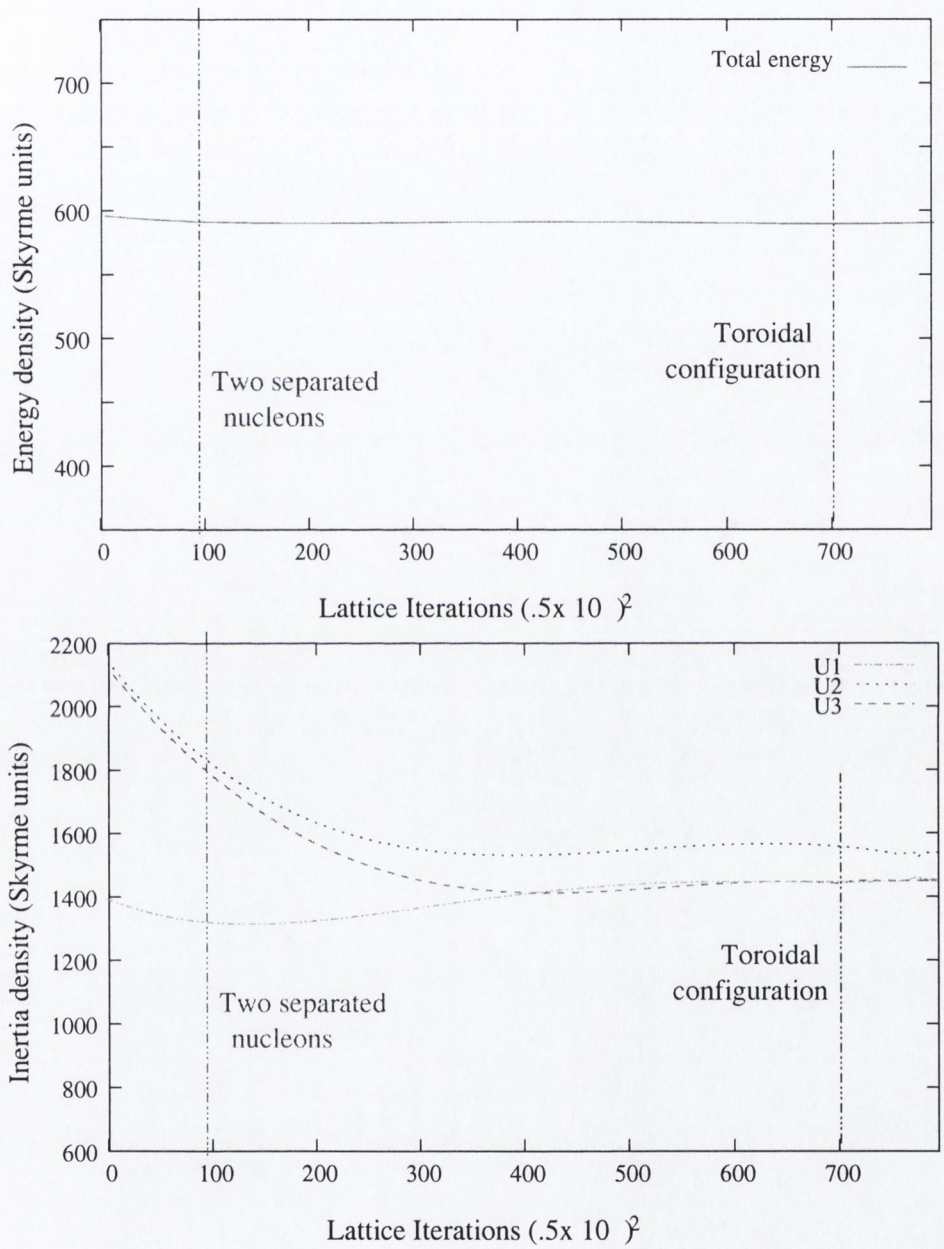

Figure 3-3: The graphs shows the evolution of the spin moments of inertia contrasted with that of the total energy during the equilibriation phase of an annealing run. The configuration being annealed is the chiral nonrotating $B = 2$ Skyrmion, starting from an initial configuration of two separated $B = 1$ hedgehogs. Polynomial fit lines extracted from thermal noise are used to show the general trend of the data. Cross-sections of the configuration at the points in the graph marked "separated nucleons" and "toroidal configuration" are shown in figure 3-2.

point, pushes close to the RAM limits of some of the processors we used, and this method would add an extra four variables. In searching for a less RAM-intensive alternative, our first idea was just to anneal until the energy converged on some value. However the example demonstrated in figure 3-2 of two well separated $B = 1$ Skyrme configurations annealed to a $B = 2$ toroid configuration illustrates the inadequacy of this approach. The difference between separated and toroidal Skyrme energies is negligible compared to the thermal noise; the thermalized energy is roughly the same for both configurations. The rotational and isorotational moments of inertia, on the other hand, change considerably in the transition from an initial structure to the final annealed structure. Therefore a more accurate measure of the stopping point is given by testing whether these inertia values have stopped changing over a certain number of lattice iterations. Also, in equilibrium, the algorithm should be accepting around 50% of those perturbations that cause a rise in energy and rejecting the rest; an additional check is performed by testing this for random points on the lattice.

3.1 Move class and cooling schedule

The Skyrme field will reach the global minimum energy configuration at the end of the annealing run provided that the temperature parameter T is lowered to zero slowly enough to allow the entire space of possible configurations to be searched. Therefore, cooling schedule governing the rate at which T is lowered is chosen to keep the system in a state of near equilibrium throughout the run.

We define the *move class* of a lattice point as the space of all possible perturbations of the point. The move class can be changed by changing the manner in which the field is perturbed, and a good move class will considerably improve the algorithm's ability to search the configuration space, enabling a shorter cooling schedule to be employed. A suitable move class is of particular importance in keeping the algorithm running efficiently at low T; if the move class remains unchanged as the temperature is lowered, increasingly fewer of the generated perturbations will be acceptable and the system will eventually spend most of its running time rejecting perturbations.

A first attempt to rectify this would be to dynamically change the length scale of the move class, reducing it if the acceptance rate is falling. This will, however, eventually lead to the system only accepting perturbations within a very small neighbourhood of a point and curtailing the latitude of the algorithm to explore the configuration space.

Instead we introduce a probability distribution to the perturbation; the width of the distribution narrows as T is lowered, making smaller perturbations more likely but still not ruling out the possibility of a large perturbation. For a given probability distribution one can often find out what type of cooling schedule will enable the algorithm to converge; a well-known case of this is the proof supplied in [39] in a study of the application of SA to image resolution, showing the convergence to the global minimum of a Gaussian probability distribution with a logarithmic cooling schedule.

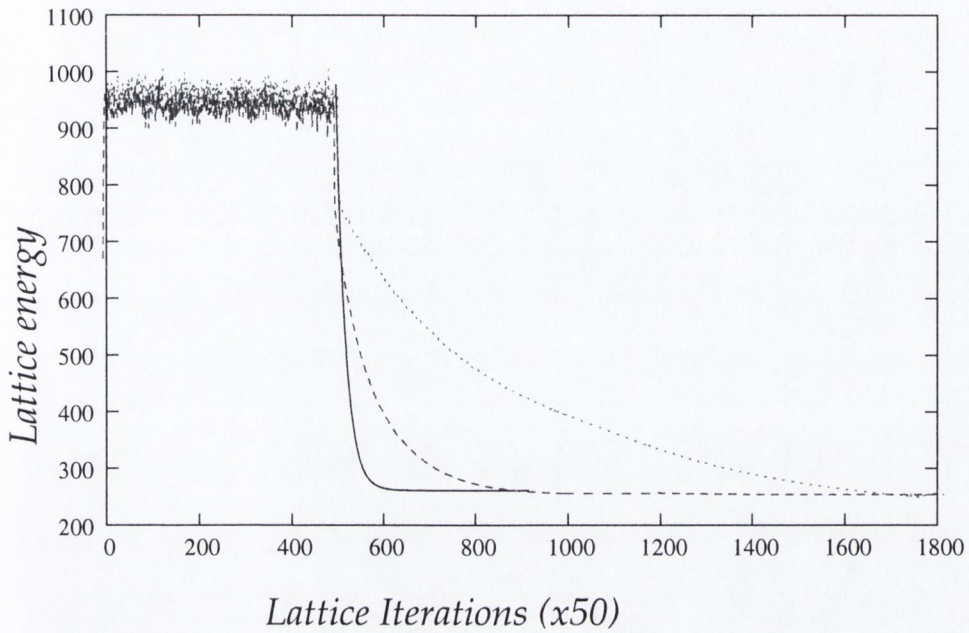

Figure 3-4: Plot showing energy of system during three separate runs, all with an equilibriation stage of 25,000 iterations. The lines correspond to the exponential cooling schedule in (3.4) with the cooling parameter c set at .004, .0004 and .0001 respectively

3.1.1 Probability distribution for the next move

We use a probability distribution that enables a much faster convergence rate developed by Ingber and described in [40]. Using this distribution, a field component U_i is perturbed to a new field component $U_i + \delta U_i$, with δU_i chosen according to

$$\delta U_i = \delta U_{max} \left(\text{sign}\,(u)\, T_d \left(1 + \frac{1}{T_d} \right)^{2u-1} \right), \tag{3.3}$$

where δU_{max} is the maximum value of δU_i set by topology considerations as described in 3.3, and u is a random number between -1 and 1. The distribution comes with its own temperature scale T_d which is independent of, but can be linked to, the acceptance temperature T. If there is no limit on δU_{max}, then the move class includes all possible values of U_i. If this is the case, the algorithm is guaranteed to converge, provided the acceptance temperature T is lowered according to

$$T = T_{init} \exp\left(-c n_a\right), \tag{3.4}$$

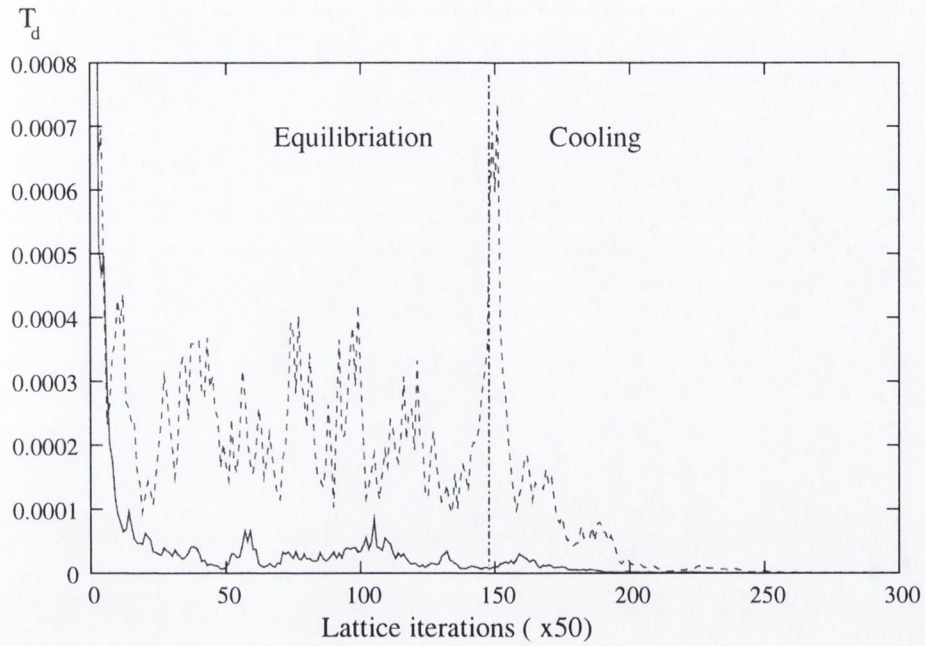

Figure 3-5: Plot showing the changes in the temperature T_d governing the ASA probability distrubution in the course of a typical simulation. Here, the temperature is increased based on perturbations of the field component U_1 at the origin (solid line) and at a point 3.6 Skyrme units outside the origin (dashed line). We see that the origin is less willing to accept perturbations; and also that T_d has roughly the same exponential decrease as T.

where T_{init} is an initial starting temperature, n_a is the number of accepted perturbations at a given lattice point and c is a tunable parameter.

Ingber uses a 'reannealing' method to modify his acceptance temperature based on the contours of the energy landscape; we adopt a simpler approach, instead aiming to keep a constant acceptance rate of about 50%. The algorithm is always more inclined to accept smaller perturbations as they cause a smaller rise in energy, and so we use the crude but effective method of raising T_d every time a perturbation is accepted and lowering T_d every time one is rejected. The end result is that T_d has much the same exponential decrease as T.

Different parts of the lattice have different sensitivities to perturbations; the near-vacuum lattice points are more ready to accept perturbations than those where substantial amounts of Skyrme matter are located. This is because the energy increase from a perturbation is greater where there is concentrated Skyrme matter than for the same perturbation where there is vacuum. To increase efficiency we assign a sep-

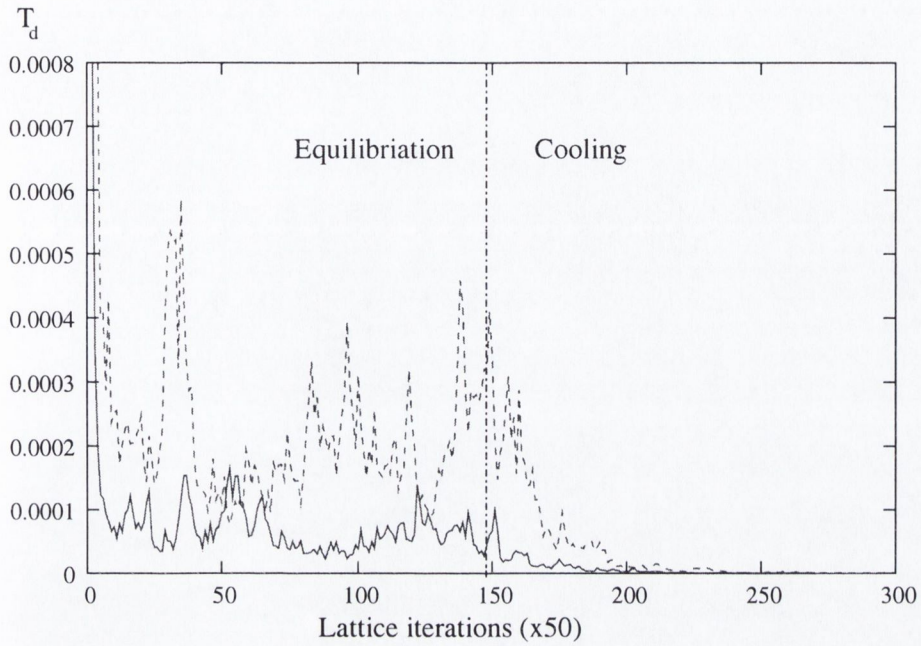

Figure 3-6: As 3-5, but with the temperature increased based on perturbations of the field component U_2 at the origin (solid line) and at a point 3.6 Skyrme units outside the origin (dashed line). We see that the U_2 component is equally sensitive to perturbations as U_1 and that it makes sense just to have one T_d governing all perturbations.

arate T_d and n_a to each lattice point. Ingber also suggests assigning a separate T_d to each component. We tried this initially, but found that our four field components U_i were roughly equally sensitive to lattice perturbation. Plots of showing the changes in perturbation temperature during a typical algorithm run are shown in figures 3-5 and 3-6.

3.1.2 Perturbing the field components

Studies of SA on functions of many continuous variables [41] indicate that, in making the perturbation, it is more efficient to perturb only one field component rather than all the components together. Further studies [42] show additional improvement if a random subset of components is perturbed. This seems to be the case in our simulations, although the difference is not as marked as for these studies which perturbed many more components. The four components U_i of the SU(2) matrix U must be perturbed such that U remains unitary, that is, such that $\Sigma_i U_i^2 = 1$. The simplest

way to achieve this is to perturb the fields as

$$U_i \to \frac{U_i + \delta U_i}{\sqrt{\Sigma_p \left(U_p + \delta U_p^2\right)}} \tag{3.5}$$

When only one point at a time is perturbed this is equivalent to the method in [43] where U_i is treated as a vector and rotated. For plaquettes, optimal acceptance occurs when all the lattice points in the plaquette are rotated the same way; we closely approximate this by perturbing the same components of each point in the plaquette with the same random perturbation.

This method is very simple to implement but has a drawback in near-vacuum fields when only one or two components are perturbed; dividing by the determinant tends to negate the perturbation and the algorithm accepts a configuration that is not much different from the original one. If a single field component U_a is being perturbed it is more efficient to carry out the unitarization as follows

$$\begin{aligned}
&U_a^{old} \to U_a^{new}, \\
&U_b^{old} \to U_b^{new} = \sqrt{\left(1 - (U_a^{new})^2\right)\left(1 + \left(\tfrac{U_c^{old}}{U_b^{old}}\right)^2 + \left(\tfrac{U_c^{old}}{U_b^{old}}\right)^2\right)^{-1}}, \\
&U_c^{old} \to U_b^{new}\left(\tfrac{U_c^{old}}{U_b^{old}}\right), \\
&U_d^{old} \to U_b^{new}\left(\tfrac{U_d^{old}}{U_b^{old}}\right),
\end{aligned} \tag{3.6}$$

where a, b, c, d are three unequal indices in the range 0 to 3. Here, the unitarization is explicitly done in such a way as to keep the perturbations intact.

3.2 Implementing energy and inertia terms on the lattice

The energy densities $\mathcal{E}$ and moment of inertia densities $\mathcal{U}_{ij}, \mathcal{V}_{ij}, \mathcal{W}_{ij}$ at a lattice point are:

$$\begin{aligned}
\mathcal{E} &= \sum_{i=1}^{3}\sum_{k=0}^{3}\left(\partial_i U_k\right)^2 + \sum_{i=2}^{3}\sum_{j=0}^{j<i}\sum_{k=1}^{3}\sum_{l=0}^{l<k}\left(\partial_i U_k \partial_j U_l - \partial_i U_l \partial_j U_k\right)^2 + 2m\left(1 - U_0\right) \\
\mathcal{V}_{ij} &= \sum_{k=0}^{3}\Bigg[\left(T_i\right)_k\left(T_j\right)_k + \sum_{l=0}^{l<k}\sum_{m=1}^{3}\left(\left(T_i\right)_k \partial_m U_l - \left(T_i\right)_l \partial_m U_k\right) \\
&\qquad \times \left(\left(T_j\right)_k \partial_m U_l - \left(T_j\right)_l \partial_m U_k\right)\Bigg] \\
\mathcal{U}_{ij} &= \sum_{k=0}^{3}\sum_{m,o,p,q=1}^{3}\epsilon_{imo} x_m \partial_o U_k \epsilon_{jpq} x_p \partial_q U_k \\
&\quad + \Bigg[\sum_{k=0}^{3}\sum_{l=0}^{l<k}\sum_{m,o,p,q,r=1}^{3}\left(\epsilon_{imo} x_m \partial_o U_k \partial_r U_l - \epsilon_{imo} x_m \partial_o U_l \partial_r U_k\right) \\
&\qquad \times \left(\epsilon_{jpq} x_p \partial_q U_k \partial_r U_l - \epsilon_{jpq} x_p \partial_q U_l \partial_r U_k\right)\Bigg] \\
\mathcal{W}_{ij} &= \sum_{k=0}^{3}\Bigg[\sum_{m,o=1}^{3}\epsilon_{imo} x_m \partial_o U_k \left(T_j\right)_k \\
&\quad + \sum_{l=0}^{l<k}\sum_{m,o,r=1}^{3}\left(\epsilon_{imo} x_m \partial_o U_k \partial_r U_l - \epsilon_{imo} x_m \partial_o U_l \partial_r U_k\right)\left(\left(T_j\right)_k \partial_r U_l - \left(T_j\right)_l \partial_r U_k\right)\Bigg]
\end{aligned}$$

where T_i is the commutator of the Skyrme field and i-th Pauli matrix τ_i as defined in (2.51). The indices i, j, m, o, p, q and r indicate spatial direction, k and l label the components U_i of the SU(2) field.

The derivatives must be approximated from the lattice field points using a Taylor expansion, shown here to first order:

$$\partial_i U\left(\mathbf{x}\right) = \frac{U\left(\mathbf{x} + h\hat{\mathbf{x}}_i\right) - U\left(\mathbf{x} - h\hat{\mathbf{x}}_i\right)}{2h} + \mathcal{O}\left(h\right)^2 \tag{3.7}$$

where h is the spacing between the lattice points. However, this approximation immediately presents a 'doubling problem': if the derivatives for the energy term

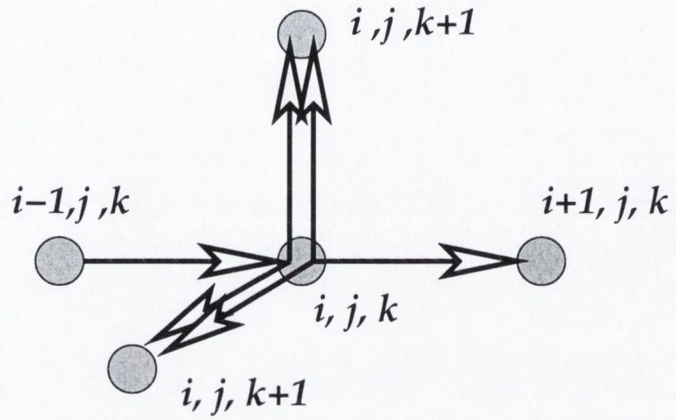

Figure 3-7: Scheme for calculating derivatives to avoid doubling. Derivatives are calculated using the measured point and nearest neighbours in each direction. Two possible ways of calculating the derivatives are shown above, each marked by triads of perpendicular lines meeting at i, j, k, the arrowheads indicate the derivative direction. There are eight such combinations; energies are calculated for each and averaged.

are written only in terms of nearest neighbours, then the derivative term at a lattice point is independent of the derivative term for its nearest neighbour. Thus, the simulated annealing algorithm will, in finding the minimum, divide the lattice into two independent lattices and find the minimum solution for each configuration. Due to the finite size of the lattice, the two solutions have slightly different boundary conditions and will not match up to each other. Using the Taylor expansion to approximate the derivative to higher orders will only mildly correlate the lattice as the nearest neighbour terms are still dominant and so the effect will remain.

The doubling problem is overcome by a derivative method that correlates the measured point with its nearest neighbours in each direction. As the classical energy is the dominant term, this correlation need be applied to the calculation of the energy densities only. We use two such methods in our simulations depending on the circumstance: local averaging and the dual lattice.

3.2.1 Local averaging

There are eight different ways of combining a lattice point and one neighbouring point along each of the three axes; two such combinations are shown in figure 3-7. From each of these combinations, derivatives in each of the three directions were approximated

using the Taylor expansion. Using these derivatives, we can then compute the energy density for each combination and average over all combinations to obtain our final answer.

Determining the local energy and inertia change arising form a lattice perturbation occupies the majority of computer time in executing the algorithm, so efficiency is quite an important consideration here. The averaging method is the less intensive of the two methods we consider, at least in the 3D case. It also has the advantage that the pion mass energy term does not have to be modified to make it doubling-free. This is the method we used for our 3D simulations.

3.2.2 The dual lattice

A method that appears at first glance to be computationally less expensive than local averaging is the dual lattice method employed in [43]. Here the energies are instead calculated at imaginary lattice points midway between the field lattice points. The field value at these 'dual' lattice points is defined as an average of the fields at the eight surrounding lattice points, and the derivatives in the i-th direction are defined as follows:

$$\frac{\partial U_l}{\partial x_i} = \frac{1}{h}\left[\frac{\sum_{j,k} U_l^{i+1,j,k}}{\sum_l \sum_{j,k}\left(U_l^{i+1,j,k}\right)^2} - \frac{\sum_{j,k} U_l^{i,j,k}}{\sum_l \sum_{j,k}\left(U_l^{i,j,k}\right)^2}\right] \tag{3.8}$$

$$\equiv \hat{U}^{i+1} - \hat{U}^i \tag{3.9}$$

This is the Taylor expansion using averaged fields on either side of the dual lattice points in place of $U(x+h)$ and $U(x-h)$; the square root factor on the bottom is to keep the averaged field unitary.

This would be computationally less demanding than the local averages method if the annealing were done without including the rotational energy terms. However, the spin inertia energy term in particular is lowered by a spreading of the Skyrme energy distribution, and in the dual lattice method the algorithm is able to 'cheat' by artificially creating field anomalies near the edge of the lattice which are partially

undetectable by the classical energy terms. It does this by creating non-zero field configurations such that both the field and the unfavourable derivatives average to zero. This can be dealt with in a simple and elegant way for the sigma model energy term [45]:

$$\begin{aligned} E_2 &= \sum_{i,l} \left(\frac{\partial U_l}{\partial x_i} \right) \\ &= \sum_{i,l} \left(\hat{U}^{i+1} - \hat{U}^i \right)^2 + \mathcal{O}(h)^2 \\ &= \sum_{i,l} \left[\left(\hat{U}^{i+1} \right)^2 - \left(\hat{U}^i \right)^2 \right] + \mathcal{O}(h)^2 \end{aligned} \tag{3.10}$$

and in a rather clumsier fashion for the pion mass term

$$E_m = 1 - \sqrt{1 - U_1^2 - U_2^2 - U_3^2} \tag{3.11}$$

However, for the Skyrme energy term one must find derivatives at each of the eight surrounding points and take averages, as in the local averaging method. When implementing unitarity on the fields is also taken into account, we conclude that the dual lattice method is more time consuming than local averaging.

For each perturbation, the local energy change on all affected points must be calculated. Therefore, the number of lattice points affected by perturbing a plaquette of n^3 points is an important consideration in determining the more efficient method. For the local averaging method, the number is n^3+6n^2, compared to $(n+1)^3$ for the dual lattice method. For $n = 1$ local averaging changes the energy of seven surrounding points compared to eight for the dual lattice; however for small $n > 1$ the dual lattice changes the energy of less points than local averaging. In our implementation, we used a maximum plaquette size of $n = 3$, so the difference is not too large; however, it is probably enough to compensate for the increased computational time of the dual lattice method.

The dual lattice has the additional advantage of being easier to implement in parallel programming. It also lends itself much more easily to the cartoon method described in section 3.4.

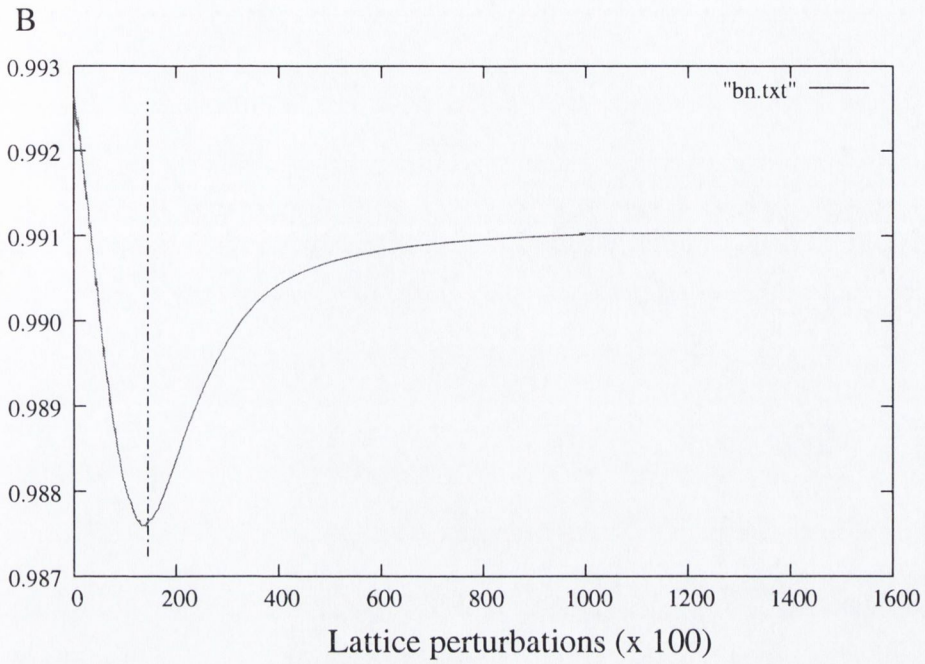

Figure 3-8: Plot of the baryon number in the course of an annealing run on a $B = 1$ configuration using a 2D 250 $\times$ 250 cartoon lattice with spacing .06. The dashed line separates the equilibrium and cooling runs.

3.3 Preserving topology

The primary restriction on the performance of the SA algorithm is given by the need to maintain the baryon number of the configuration. In the continuum theory, the baryon number B, equated to the winding number of the solitonic configuration, is a constant regardless of changes in the shape of the configuration. In the discretized lattice space which approximates the continuum, however, the numerics of the algorithm can break down for sharply fluctuating fields because the Taylor approximation (3.7) is not able to accurately calculate the derivatives. There is therefore a possibility that the configuration can lose its winding number and end up at a vacuum final state.

The temperature T governs the extent to which the lattice points fluctuate thermally; there is therefore a limit on the maximum initial temperature T_{init} one can use during the equilibriation stage. On the other hand, we must ensure that this temperature is high enough so that the energy of the thermalized configuration rises above that of the energy barriers separating local and global minima. This is achiev-

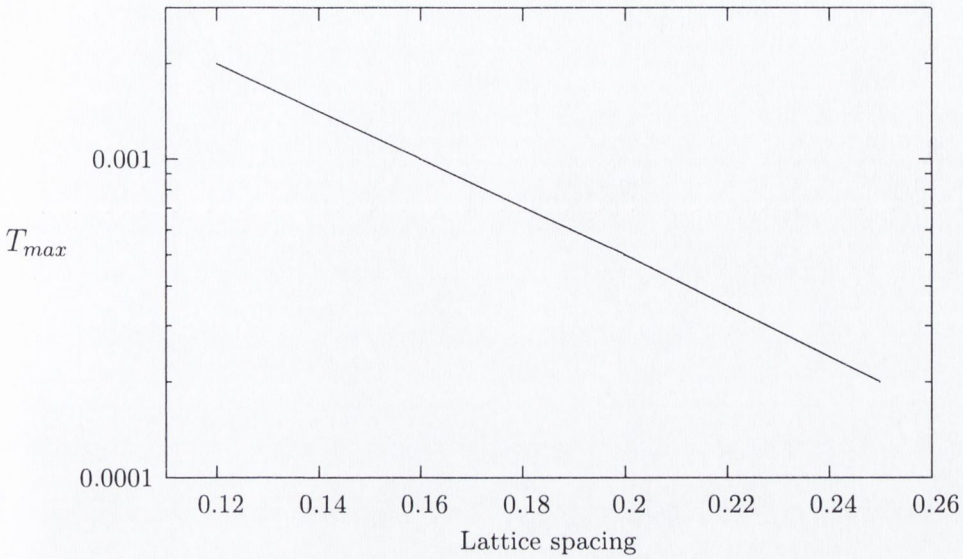

Figure 3-9: Logarithmic plot of the maximum annealing temperature T_{max} above which the topology of the Skyrme configuration is lost, as a function of lattice spacing in Skyrme units $2/eF_\pi$.

able provided appropriate values of the maximum perturbation length and lattice spacing are chosen. An over-long perturbation length δU_{max} governing the move class allows fluctuations in the configuration that the Taylor approximation cannot handle. Therefore, in all our runs, δU_{max} is kept at .03. This, of course, means that the cooling schedule (3.4) no longer gives a cast-iron guarantee of convergence and we must tune the constant c to ensure the system cools slowly enough. The largest lattice spacing we use is .12; this gives a maximum value of T_{init} of .002. This is the same temperature that produced good results in [43, 21]; it typically gives an equilibrium energy around fifteen times that of the final configuration.

3.4 The Cartoon Method

The main thrust of our work is finding minimum energy Skyrme configurations without any prior symmetry assumptions. However if an annealed solution were shown to have a particular symmetry, we could then use that symmetry in another implementation of the SA algorithm which lessens the computer workload and produces more accurate results. With specific reference to the B=1 and B=2 Skyrmions, if the Skyrme fields were shown to have axial symmetry, we could then obtain more accurate results by annealing on a 2D grid.

In the axially symmetric case, the inertias U_{ij}, V_{ij} and W_{ij} simplify to four independent inertias: U_2, V_2, V_3 and W_2. A 2D simulation arranges the Skyrme fields such that we can calculate the local energy and inertia values on a plane radially jutting out from the cylinder axis. We express this plane as $(r, \phi = \phi_0, z)$ in cylidrical polar coordinates.

We can calculate the energy and inertias of the full 3D configuration using the local transformation properties of the energy and moment of inertia densities $\mathcal{E}, \mathcal{U}_2, \mathcal{V}_2, \mathcal{V}_3$ and $\mathcal{W}_2$ under cylindrical symmetry:

$$\begin{aligned} \mathcal{E}(r, \phi_0 + \phi, z) &= \mathcal{E}(r, \phi_0, z) \\ \mathcal{V}_3(r, \phi_0 + \phi, z) &= \mathcal{V}_3(r, \phi_0, z) \\ \mathcal{V}_2(r, \phi_0 + \phi, z) &= \mathcal{V}_2(r, \phi_0, z)\cos^2\phi + \mathcal{V}_1(r, \phi_0, z)\sin^2\phi \end{aligned} \tag{3.12}$$

The other axially-symmetric inertia densities of interest, $\mathcal{U}_2$ and $\mathcal{W}_2$, transform in the same manner as $\mathcal{V}_2$. Thus the classical energy (2.13) and moment of inertia (2.51) integrals over $\mathbb{R}^3$ change to the following integrals over the (r, z) plane once ϕ is integrated out:

$$\begin{aligned} E &= 2\pi \int \mathrm{d}r\,\mathrm{d}z\; r\,\mathcal{E}(r, z), \\ V_3 &= 2\pi \int \mathrm{d}r\,\mathrm{d}z\; r\,\mathcal{V}_3(r, z) \\ V_2 &= \pi \int \mathrm{d}r\,\mathrm{d}z\; r\,\mathcal{V}_1(r, z) + \mathcal{V}_2(r, z) \end{aligned} \tag{3.13}$$

Thus when a point $(r, \phi = \phi_0, z)$ is perturbed in the SA algorithm, the change in the energies and inertias arising from the perturbation is calculated using the integrands in (3.13).

However, using cylindrical coordinates in our simulations on the 2D grid invariably leads to singularities which are difficult to work around, whereas 3D cartesian coordinates have no such complications. The trick is to do the simulation in Cartesian coordinates using a thin 3D slab positioned so that the points where the energies and inertias are calculated lie at $\phi = \phi_0$. The slab is thick enough so that the derivatives in the $\boldsymbol{\phi}$ direction can be calculated; the dual lattice method only needs a slab two points thick. The energies and inertias thus obtained are then integrated to find the total energy.

In our implementation, the $(r, \phi = \phi_0, z)$ plane is coincident with the $(x = 0, y, z)$ plane, so that $|\mathbf{y}| = r$ and $\hat{\mathbf{x}} = \boldsymbol{\phi}$. The lattice field points are arranged as in figure 3-10, so that the $(x = 0, y, z)$ plane is the plane of dual lattice points on which the local energies and inertias are calculated. There are thus two (y, z) planes of field lattice points located at $x = \pm h/2$, where h is the lattice spacing. The (y, z) lattice plane at $x = h/2$ is swept, and each time a point is perturbed, its counterpart at $x = -h/2$ is also updated by rotating the field at $x = h/2$. The new values for both points are then accepted or rejected according to the Metropolis criterion (3.2).

The 'cartoon method' [47], as it is called, is ideally suited to the dual lattice discussed in section 3.2. An implementation using local averaging would require three planes of field points, at $(x = 0 \text{and} \pm h, y, z)$; the values of the points not on the centre plane would have to be interpolated from the points on the centre plane using trigonometric identities. However the dual lattice implementation has no such problem; the values of the field components at $(-h/2, y, z)$ are just plus or minus those at $(h/2, y, z)$, depending on the component.

It is necessary to perturb the field such that axial symmetry is preserved; this can be done by keeping U within the ansatz

$$\begin{aligned} U_0 &= \bar{f}_0, & U_1 &= \bar{f}_1, \\ U_2 &= \bar{f}_2 \cos\phi, & U_3 &= \bar{f}_2 \sin\phi, \end{aligned} \tag{3.14}$$

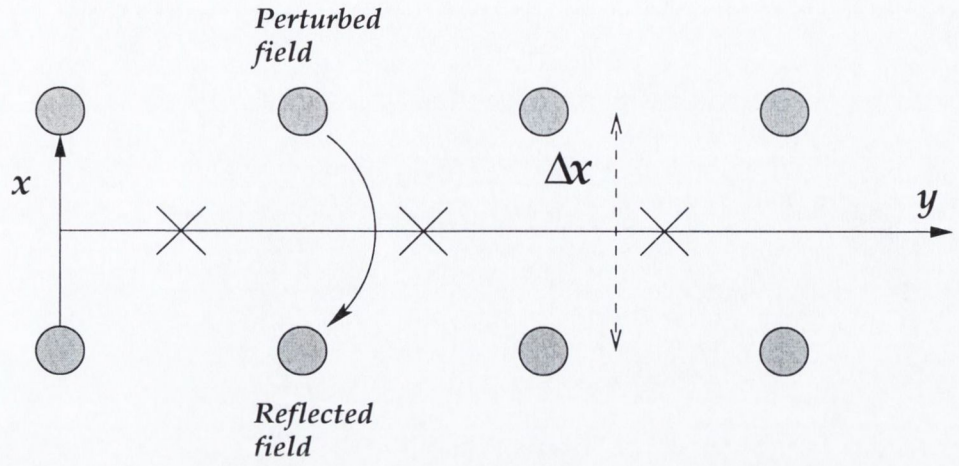

Figure 3-10: Schematic of dual lattice cartoon method with z-direction compressed. The field lattice points (shaded circles) at z and $z+1$ are located on top of each other, and the dual lattice points (crosses) are on the $z+1/2$ plane.

where $\bar{f}_0, \bar{f}_1, \bar{f}_2$ are functions of $f(r,z)$ such that $\Sigma_i \bar{f}_i^2 = 1$. This has the effect of permanently fixing B, as on the $x = \pm h/2$ planes U_2 and U_3 are kept in a constant ratio to each other; for the cartoon method we can make the maximum perturbation length as large as we wish.

3.5 Method evaluation and suggested improvements

Most of our 3D annealing runs were performed on a 90^3 lattice with 8 parallel CPU's, the lattice being divided into 45^3 subcubes and a CPU assigned to each subcube. This arrangement meant we could then perturb a spherical lattice of radius 45, reducing the computational workload by a factor of $\pi/6$, whilst still spreading the load equally amongst all processors. The Taylor expansion used for the derivative (3.7) meant that we had to pass on the values of the fields at the borders between subcubes to neighbouring processors. However, the fields were only updated and passed on after each full lattice iteration, and so the communication between processors took a tiny fraction of CPU time compared to the computation.

The largest lattice spacing we used was .12 for the $B = 8$ and $B = 9$ cases. This spacing was in line with two previous 3D annealing simulations [43, 21], both of which which used lattices of 80^3 and modelled Skyrmions of charge one to four. In our case, the addition of large pion masses contract the configuration; a $B = 8$ minimum energy solution with sufficiently high pion mass is around the same size as a $B = 4$ solution with zero pion mass. The pion fields also fall away more sharply towards the vacuum; for example, the $B = 1$ profile function with pion mass decreases exponentially as opposed to a $1/r^2$ decrease in the massless case. We use vacuum boundary conditions rather than the periodic conditions imposed in the previous simulations; in hindsight, periodic boundary conditions seem to result in smaller finite lattice errors as the fields are continuous at the boundary, and our finite lattice error seems to be 1% greater than that obtained in the other two simulations.

A primary requirement of the SA algorithm is that it be able to find minimum energy configurations even if they are shaped very differently to the initial starting configuration. To achieve this, our implementation sometimes requires a long equilibriation phase depending on the initial configuration. For example it may take two separated hedgehog configurations up to 20,000 lattice iterations before they coalesce into a toroidal configuration.

In the case of an initial configuration of separated hedgehogs, we note Skyrme's original observation [4] that at long range the interaction between two separated

hedgehog configurations is very similar to that between dipoles, and an initial configuration of separated Skyrmions must therefore rotate to a maximally attractive configuration before coalescing. This the rotation is equivalent to tracing a path in the energy landscape with an almost flat slope. Landscapes such as these, where the energy minimum hollows have wide tails and relatively narrow half-widths, seem ideal for an increasingly-used technique called 'basin-hopping' [48].

In this technique, the move class is such that the perturbed configuration is likely to be in a different local minimum hollow. A deterministic minimizer is then used to find the local minimum; an efficient minimizing algorithm like conjugate gradient or steepest descent can be employed here to speed up the process. The configuration is then accepted or rejected by inserting the energy of the local minimum into the Metropolis probability (3.2). The space of possible solutions is thus restricted to the space of local minima. It would be impossible to adapt the move class in our implementation such that the configuration can be perturbed to a different local minimum hollow; instead, a good approach would be to generate a rational map ansatz using a random rational map of degree B.

Our implementation was capable of annealing configurations with large pion mass up to $B = 9$, but extensive computational improvements must be made in order to anneal configurations with higher baryon number. Our current lattice size is the largest that can generate solutions in a reasonable time; a thorough simulation of 25,000 equilibriation iterations followed by cooling with a parameter c=.0002 takes almost one week on eight 3MHz processors. The computing time increases as the cube of the lattice size, hence an increase of even ten points per subcube on our current value will double the computing time.

One option is to increase the lattice spacing, particularly if finding the structure is more important than getting an accurate minimum energy. As we discussed in section 3.3, any increase in the lattice size rapidly lowers the maximum temperature at which we can anneal and still keep the topology intact. This effect is exacerbated for high pion masses, which contract the configuration and cause high derivative gradients. One way of keeping the winding number is to add a Lagrangian multiplier

λ [21] to constrain the baryon number to its correct value B:

$$E \to E + \lambda \left\langle \left(\int \mathrm{d}^3\mathbf{x}\, \mathcal{B} \right) - B \right\rangle^2 \tag{3.15}$$

The energy E and the Skyrme configuration space $\mathcal{Q}$ cannot be parameterized in terms of a common variable, and so λ cannot be computed directly. The simplest method is to tune λ to the problem at hand using trial and error. The resulting objective functions are known as *static-penalty formulations*, and they tend to make the configuration space more rugged and deepen the local minima with increasing λ. In our case, it appears at first sight to be a rather costly method for lattice acceptances. As the fields become thermalised, the accuracy of the Taylor approximation decreases slightly, and there is a slight lowering in the baryon density. As seen in figure 3-8, the baryon density will later be recouped in the cooling as the thermal noise is eliminated and the fields become smoother. A tight constraint on the baryon density during the equilibriation stage might inhibit the algorithm's ability to make large moves.

A better alternative would be to set λ dynamically, so that it takes quite a low value during equilibriation and then increases as the acceptance temperature drops. An ideal value of λ can be adaptively found as the run progresses by changing the annealing problem to one of finding a configuration that simultaneously minimizes E and maximizes λ [49]. The annealing search is thus extended to a direct product of the Skyrme configuration space and the 1D space parameterised by λ.

One easy way to anneal larger configurations is to rescale the unit of length. Our unit of length is set at $2/eF_\pi$; a length of $2\sqrt{2}/eF_\pi$ is used in [21] to cater for the expansion of the configuration under the influence of sixth and eighth order Skyrme terms. However, we have the opposite problem; the contraction of the configuration with the addition of a pion mass means that our current length unit is close to the outer limit beyond which the numerics no longer model the solution accurately. However, a large length unit is certainly a good starting point to get an idea of the structure of higher charge Skyrmions.

As regards getting accurate results, the only real option is to increase the number

of processors to 64 or more. At the time of writing, the facilities to cater for such large jobs are beginning to come onstream. In this case it would be still nice to keep the spherical lattice and spread the workload equally among all processors. Perhaps one way of doing this would be to divide the lattice into eight subcubes as we do now, and then within each subcube assign a CPU to a subgrid of uncorrelated points. This method would also have the advantage that one would be able to increase the number of processors in multiples of eight, by adding extra subgrids, rather than in integer cube powers. This method would involve considerably more communication between processors at the end of a lattice iteration; however, we suspect theat the communication to computation ratio will still be very small.

Chapter 4

Minimum energy Skyrme configurations

As a result of our simulations, we now have a comprehensive description of Skyrme configurations with high pion masses, and with quantized spin and isospin degrees of freedom. The $B = 1$ Skyrme configuration has long been the testing ground for zero mode quantization; here we present results that are perhaps counterintuitive from a classical point of view but make sense from a quantum perspective. We use the $B = 8$ configuration, whose ground state has no rotational energy, as our principal testing ground for probing the nature of the deformations from the classical minimum with high pion masses, before examining their effect on other charges. We evaluate the effect of spin and isospin degrees of freedom on configurations of baryon number up to nine. Perhaps one surprising aspect of our research is the discovery that Skyrme configurations with spin energy lower their total energy by ejecting matter towards the edge of the lattice; we investigate whether the configuration loses all its spin energy in this manner.

The chapter is structured as follows: first, we present results arising from our exploration of pion mass effects. We then discuss the effect whereby matter is ejected from spin energy configurations, before going on to discuss particles for which this effect occurs.

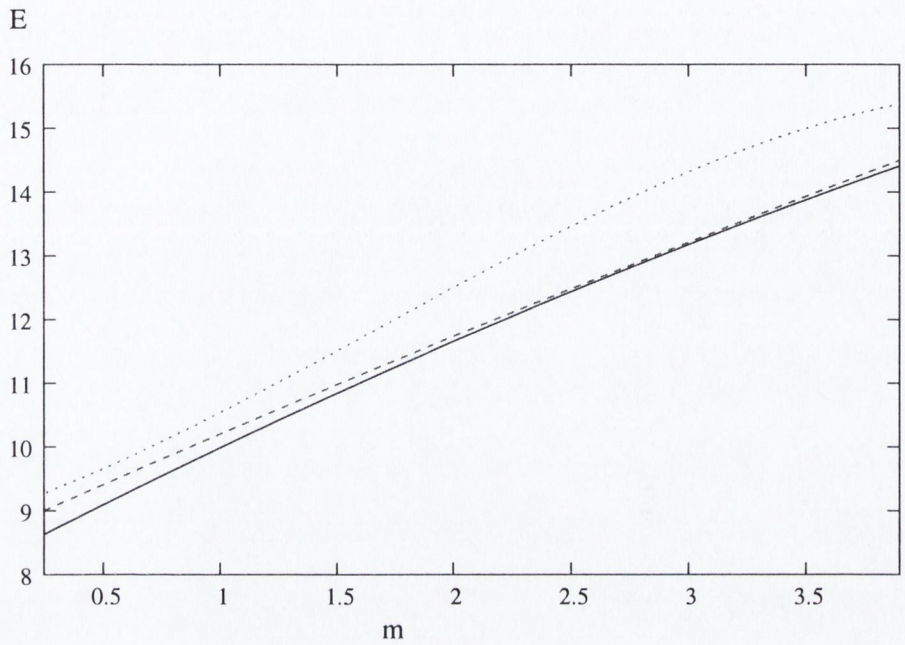

Figure 4-1: Plot comparing the energies as a function of the scaled pion mass m of a $B = 8$ annealed configuration (solid line), two well separated $B = 4$ configurations (dashed line), and the $B = 8$ rational map ansatz. The energy is divided by a factor of $12\pi^2$ for comparison with the Bogomol'ny bound (2.24).

4.1 Investigating the effect of the pion mass

For a long time, it was generally thought that any modifications to the shell-like structure of the classical minima described in Chapter 1 would be brought about by the addition of rotational terms to the Skyrme Hamiltonian. However, it has recently been suggested [16] that the pion mass term, previously thought only to localize the configuration and change its radial length scale, may have a considerable impact on the Skyrme configuration structure, and may lead to the baryon density of the minimum energy configuration becoming more equally distributed throughout the configuration volume.

We are particularly interested in one example studied in [16], in which the energy of the $B = 8$ rational map configurations was found to be higher than the energy of two $B = 4$ rational maps above a critical value of m_π. Similarly, a value of pion mass existed above which the energy of the $B = 5$ rational map solutions was higher than the combined energies of the $B = 4$ and $B = 1$ rational map solutions. This suggested

that the rational map that approximated the $m_\pi = 0$ minimum energy configuration did not accurately describe minimum energy configurations with pion masses for both values of baryon number. This result opens up a number of possibilities: the minimum energy configuration may be described by a different rational map, or it might have a distorted shape not described by any rational map; perhaps there are no bound Skyrme configurations for $B = 5$ and $B = 8$, just as there are no stable isotopes with these baryon numbers in nature. So far, nothing is known about the structure of these minimum energy configurations, but in simulated annealing we have the perfect tool to find minimum energy solutions with pion mass so their structure can be seen.

The $B = 8$ configuration, in particular, is a good testing ground to see what actually happens to the shell-like structure of a Skyrmion as the pion mass is increased from $m = 0$, where m is the scaled pion mass $2m_\pi/F_\pi e$. Both it and the $B = 4$ Skyrmion have no rotational energy term, so we can test the stability of the $B = 8$ configuration against decay into two $B = 4$ configurations independently of rotational effects.

We used simulated annealing to find minimum energy $B = 8$ and $B = 4$ solutions for different values of m ranging from $m = 0.25$ up to $m = 4$. From the graph in figure 4-1, we can see that the energy of the $B = 8$ annealed configuration approaches that of twice the annealed $B = 4$ configuration as m increases up to four times its experimental value. This is roughly the point where the energy of the $B = 8$ rational map overtakes that of twice the energy of the $B = 4$ map [16]. However the $B = 8$ energy stays below that of the $B = 4$ energy for higher values of m, proving that the annealed $B = 8$ solution is bound against breakup into two annealed $B = 4$ solutions, at least up to a pion mass value of $m = 4$. The two energies are very close together for values of $m > 2$, perhaps even within experimental error of each other; however the energy of the $B = 8$ configuration is likely to be affected more by finite lattice effects than the $B = 4$ configuration, and thus the energy difference is probably slightly greater than the graph suggests. Baryon density isosurface plots of the $B = 8$ configuration for a range of pion masses are shown in figure 4-2. We see

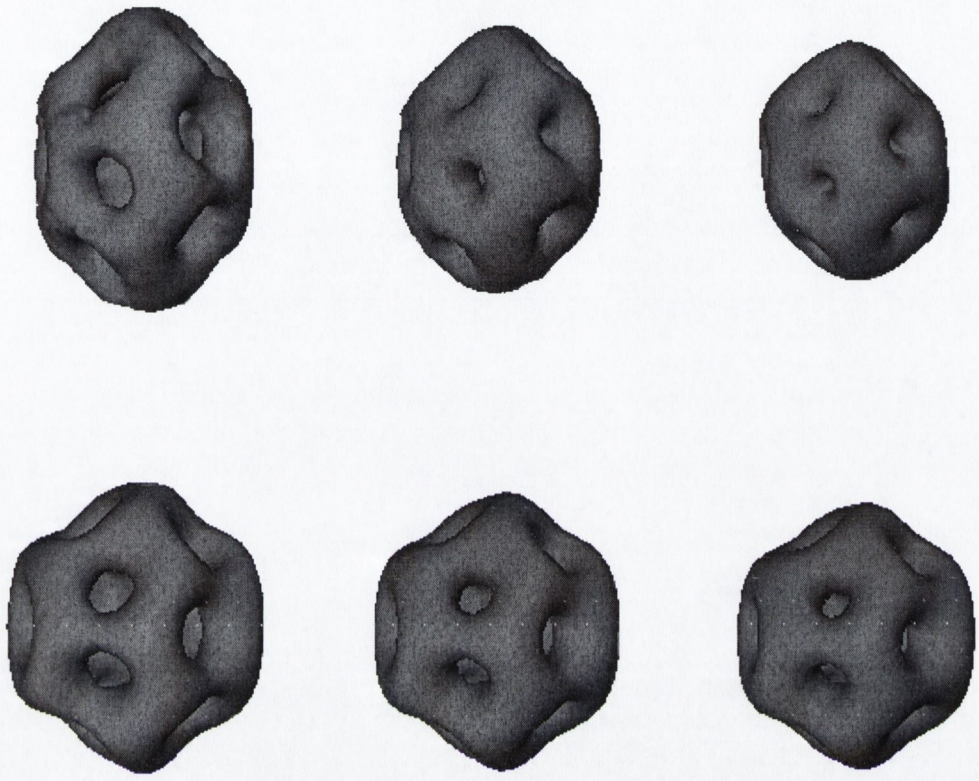

Figure 4-2: Baryon density isosurface plots at $\mathcal{B} = .017$ for pion masses at m=1.6, 3.8 and 5. These simulations were performed on lattices with spacing $h = .12$. The upper row are the annealed solutions, whilst the bottom row are their corresponding rational maps.

that the baryon density is no longer concentrated around a spherical shell, but rather a spheroidal shell whose thickness increases with pion mass. We have described in chapter 1 how Skyrme configurations for $m = 0$ are shaped like skeletal polyhedra; in the case of $B = 8$ we see that, under the influence of pion mass m, the two hexagonal faces of the polyhedron get pulled in towards the origin more than the other pentagonal faces.

This contrasts with the result of our SA simulations for $B = 7$ shown in figure 4-3: we see that the baryon density is still distributed around a spherical shell. The annealed solution is very similar to the rational map solution, albeit with slightly thicker shells. However for $B = 9$ the difference between annealed and rational map

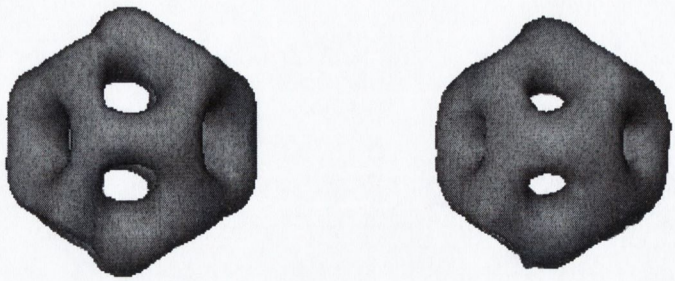

Figure 4-3: Baryon density isosurface plots for $B = 7$ at $\mathcal{B} = .025$ for a pion mass of m=3.8. The solution on the right is compared to the rational map on the left.

solutions is much more marked. The $B = 9$ solution for $m = 0$ is unusual in that it is one of the few minimum energy configurations to have four-valent vertices; it has two such vertices opposite each other. With the addition of pion mass, these four-valent vertices are pushed in towards each other to the extent that the four pentagonal faces joined together at each vertex are almost coplanar, as can be seen in figure 4-4.

We made comparisons of the $B = 4$ and $B = 5$ annealed solutions with their respective rational maps; from our combined results, we see that for the Platonic shapes of $B = 4$ and 7 the solution differs only in scale to the minimum solution for $m = 0$, and that the annealed solution is indeed a good approximation to the rational map. Changes to the configuration shape change occur for the non-Platonic shapes $B = 5, 8$ and 9; there seems to be a relationship between the number of vertices on a polygonal face of the polyhedron skeleton around which the baryon density is distributed and the extent to which that face is pushed in towards the origin under the influence of pion mass. For example, the two hexagonal faces of the $B = 8$ fullerene get pulled in more than the other pentagonal faces, and the square faces of the $B = 5$ configuration are pulled in more than the triangular faces. This is consistent with the lack of shape change in Platonic configurations; for example, the twelve identical pentagonal faces of the $B = 7$ are all pulled in equally towards the origin. The $B = 9$ polyhedral skeleton also consists wholly of pentagons, however the four-valent vertices mean that the baryon density is not distributed evenly throughout the polygonal faces. It is worthwhile noting that the $B = 9$ solution is very closely

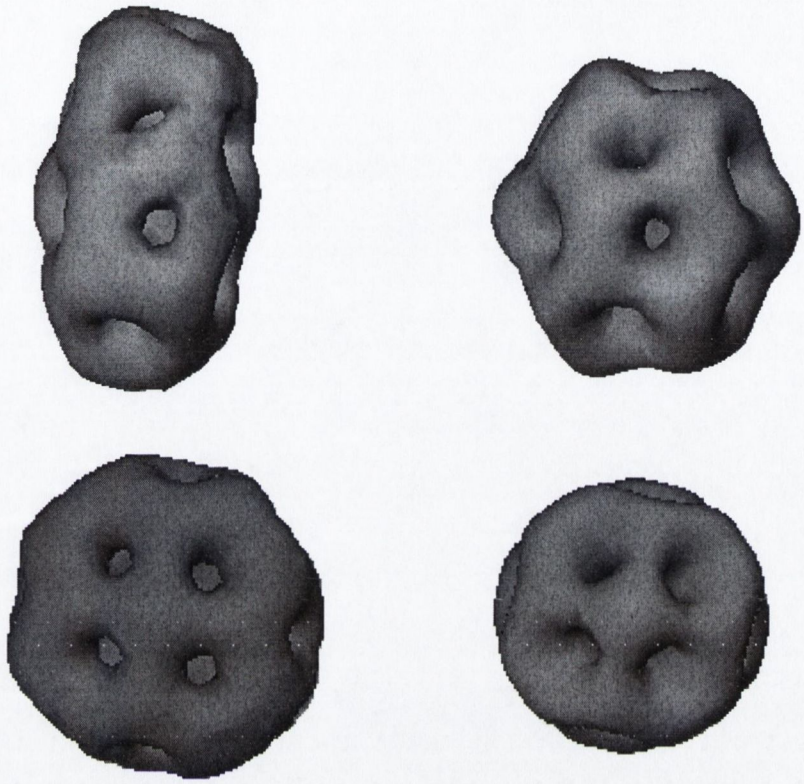

Figure 4-4: Baryon density isosurface plots for $B = 9$ at $\mathcal{B} = .025$ for a pion mass of m=3.8. The plan and elevation of the solution on the left is compared to the rational map on the right.

related to another solution in which the four pentagons are replaced by two hexagons and two pentagons [11], and that the baryon density distribution of our annealed solution is probably quite similar to the density distribution of that solution.

Finally, we investigate whether the annealed non-Platonic solutions can still be described using the rational map ansatz. A simple way of testing this is to see whether the profile function $f(r)$ used in the field ansatz (2.29) is spherically symmetric for our annealed solutions. Cross-sections of the profile function for the $B = 9$ solution are shown in figure 4-5; we see that in fact the profile function has a spheroidal distribution which matches that of the shell around which most of the baron density is distributed. One could still construct a rational map using such a profile function; however, minimizing a non-spherically profile function would require a time-consuming 3D simulation. This negates the main advantage of the rational map

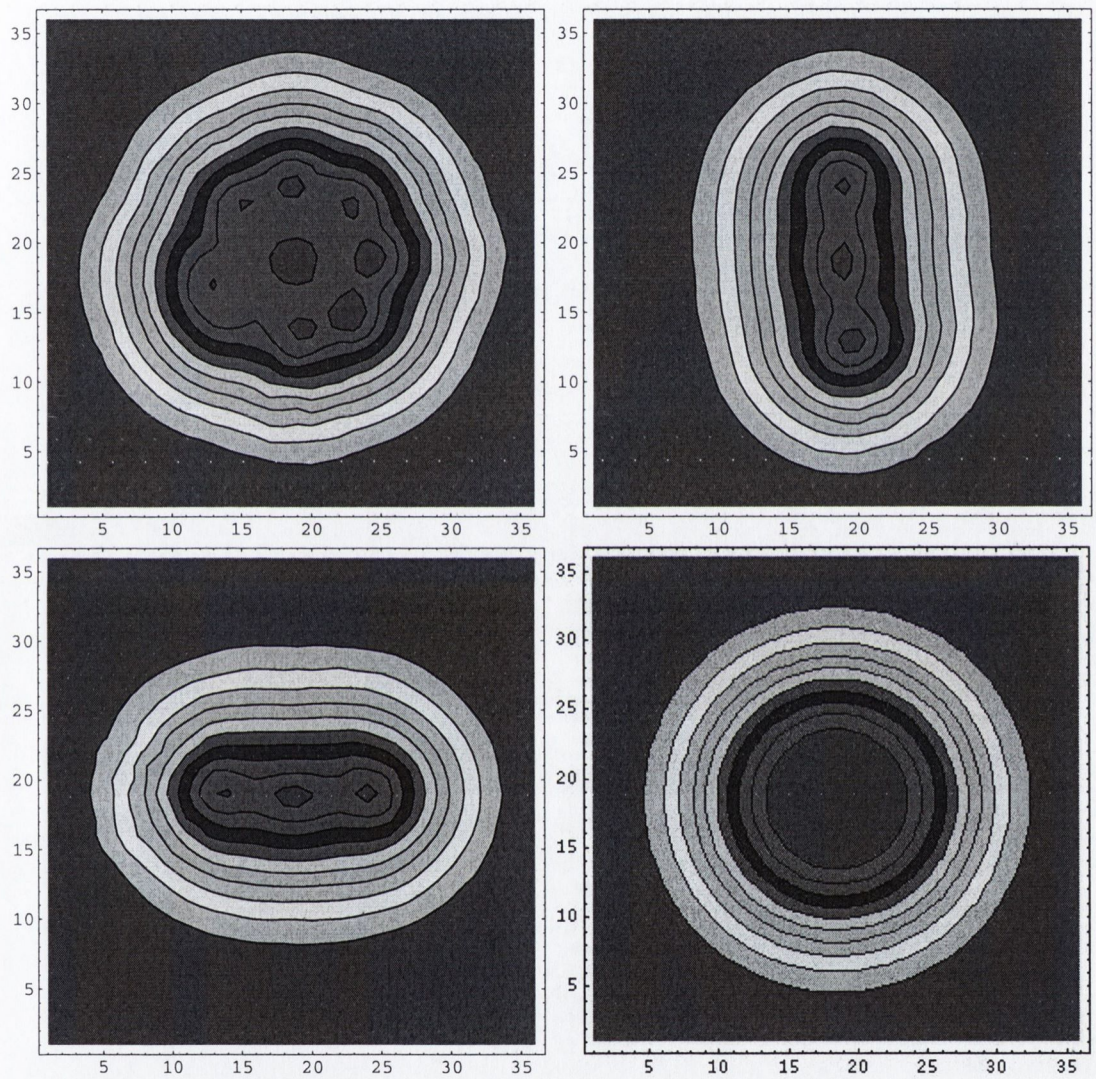

Figure 4-5: Contour plot of the profile function of an annealed $B = 9$ configuration with $m = 3.8$. The first three plots are cross-sections through the origin in the x, y and z directions, while the plot in the bottom right hand corner is the cross-section for the rational map configuratiin the x, y and z directions.

ansatz, namely that it is a fast way to generate good approximations to minimum energy solutions.

4.2 Ejected matter solutions

As described in section 2.5, the simulated annealing algorithm provides a means of obtaining the definitive zero mode quantized Skyrme configurations. We performed many simulated annealing runs for baryon numbers up to 9 with different values of spin quantum number l.

The major feature encountered in the investigation of solutions with spin energy was the discovery of *ejected matter solutions*, that is, Skyrme configurations in which some of the baryon density ends up at the very edge of the lattice boundary. An accumulation of baryon density as far away from the origin as possible lowers the rotational energy by increasing the spin moments of inertia U_{ij} by a factor of $(l/4)^2$ times the resulting increase in the Skyrme mass E, where l is the lattice size. Only a tiny fraction of the total matter is ejected, and the overall shape of the configuration does not change.

Many Skyrme model approaches have taken the view that spin and isospin moments of inertia have the same general characteristics. Much of the important work on quantizing the Skyrme model took place within a spherically symmetric ansatz which constrain the spin and isospin moments of inertia to be equal to each other and prevents ejected matter solutions by keeping the pion fields in a constant ratio to each other. Because of this assumption, the general expectation has been that any instability caused by spin energy is of the type described in section 2.4, and could thus be cured by the addition of a suitably high pion mass. This seems like a reasonable expectation, since both the spin and isospin rotational energy terms scale as $E_{rot} \rightarrow \lambda^3 E_{rot}$ as $U(\mathbf{x}) \rightarrow U(\lambda \mathbf{x})$, and the pion mass energy term scales as $E_\pi \rightarrow 1/\lambda^3 E_r$. However, the effect persists for a range of pion masses far higher than those used in [29] to produce stable isorotating solutions. In fact, the ejected matter becomes more apparent with higher pion mass since the resultant configurations have less inertia and more spin energy. Also, the instability described in section 2.4 is not

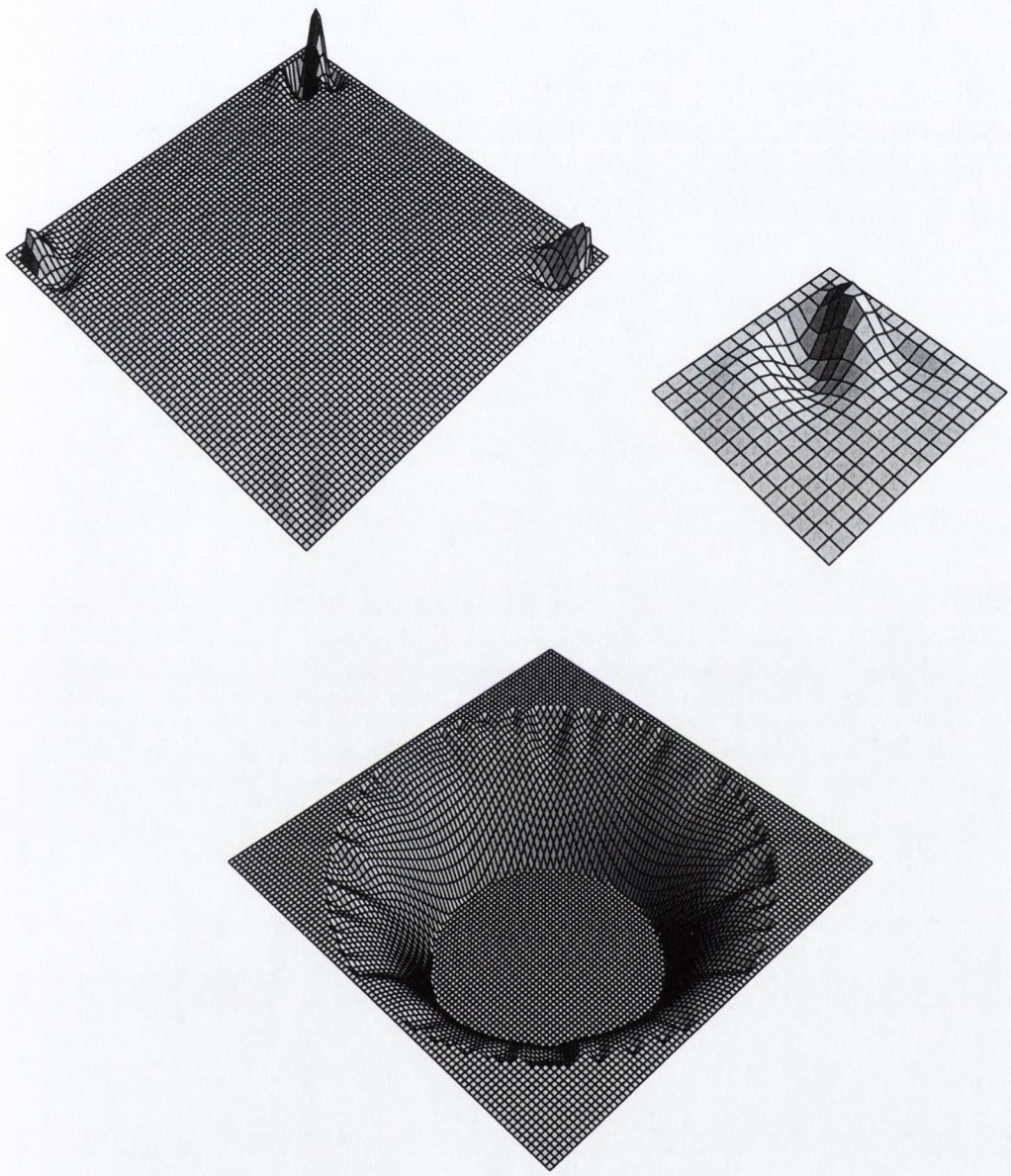

Figure 4-6: Cross-sections of the U_1 field component for a $B = 1$, spin 3/2, isospin 3/2 Skyrmion annealed using a cubic lattice (top) and spherical lattice (bottom). The cubic cross-section is taken near a cube face. The origin in this annealing run was moved slightly away from the corner where the largest concentration of matter is, showing that the configuration lowers energy by ejecting Skyrme matter as far away as possible. A close-up of the largest matter concentration is shown to the right. The spherical cross-section is taken through the origin; the Skyrme field has been truncated at $U_1 = -.002$ in order to see the effect more clearly.

visible on finite lattices; to determine whether or not a configuration is stable, one must check if the energy changes when the lattice size is varied. The spin contribution to the rotational energy term is responsible for a class of instability that cannot be controlled by the pion mass term and which are visible on finite lattices.

Obviously, upon discovery of such an effect, attention first turns to verifying the soundness of the algorithm implementation. The first, and most serious question, is whether the field and derivative definitions on the lattice are termed in such a way that the minimum energy configuration is unphysical; ways in which this might happen were discussed in section 3.2. The telltale indicator would be evidence that the instability occurs on the level of the lattice spacing; probing the structure of the ejected Skyrme matter for lattice-scale artifacts and verifying that the solution is the same when annealed with different lattice spacings are convincing ways to remove such doubts.

Once it is verified that the algorithm is working properly, the next task is to determine if the annealed configuration is indeed the minimum energy. The bulk of our tests focused on the $B = 1$, spin 3/2, isospin 3/2 Skyrmion modelling the delta resonance, enabling smaller lattices, use of the cartoon method and easier generation of multiple initial configurations. We minimized many initial $B = 1$ configurations using a 'quenching' variant of SA that only accepts perturbations of lower energy, to find that they all had ejected matter configurations as their local minima. We therefore annealed using very small lattice over as many lattice iterations as it took to bring two separated Skyrme configurations together, and came to the conclusion that the ejected energy is not merely trapped in a local minimum configuration, that it is in fact the global minimum.

So, what does what we are seeing corresponding to physically? Simulated annealing is a rather limited tool to use in answering questions of this nature. The heating and cooling in the algorithm are not steps in time; SA can give a minimum energy configuration, but it cannot illustrate the dynamical process by which it arrived there from the initial configuration. However, a shrewd investigation of the energy traces left by the process on the annealed configuration can piece together a good picture

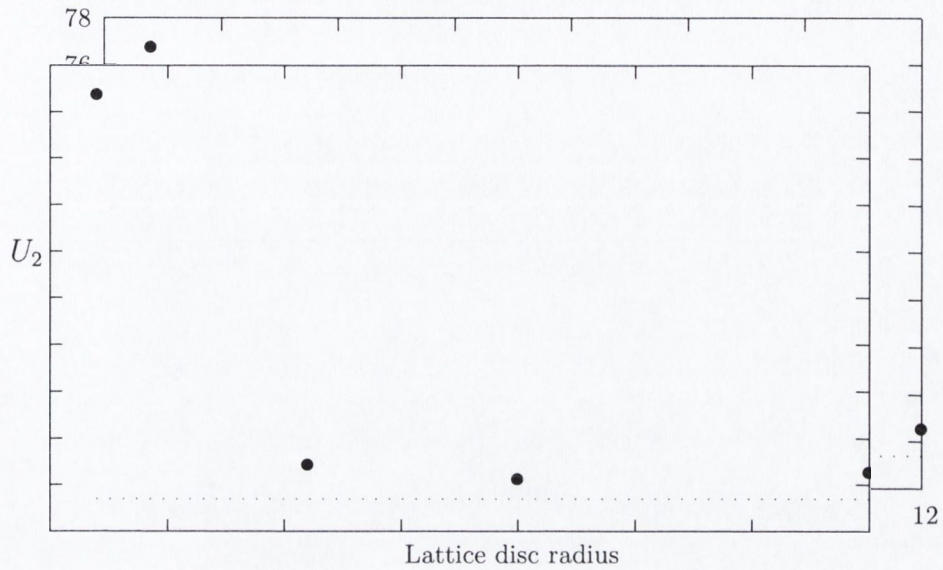

Figure 4-7: Plot showing values of U_2 for the $B = 1$ spin 3/2 isospin 3/2 minimum energy solutions annealed using the cartoon method, as a function of lattice disc radius. The line at the bottom of the graph is the value of V_2 for the simulations.

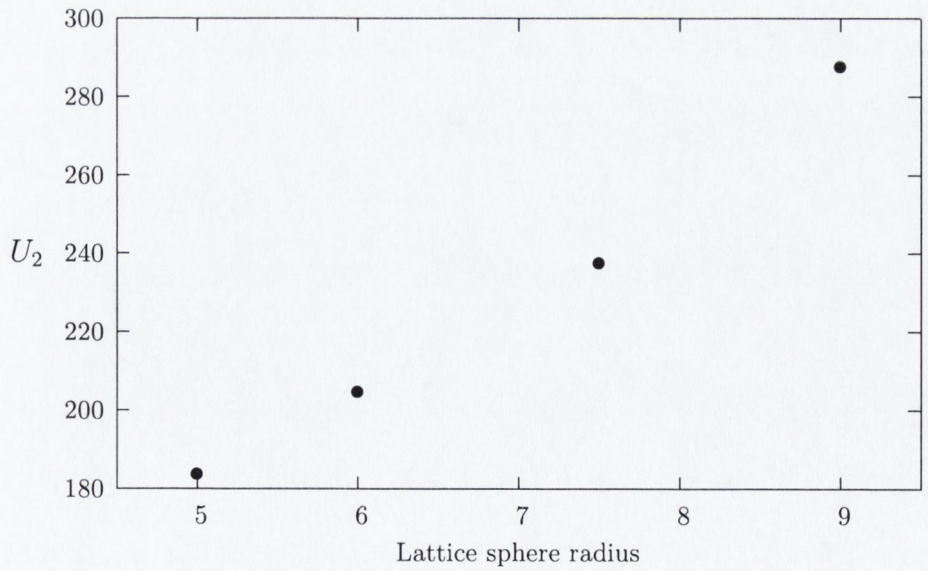

Figure 4-8: Plot showing values of U_2 for the $B = 2$ spin 1 isospin 0 minimum energy solutions obtained by 3D annealing, as a function of lattice disk radius. The simulations were done with a lattice spacing of 0.2.

of what has happened. For example, we cannot see baryon density being ejected from the main body of the configuration; however we can conclude that matter is being ejected because the baryon density is constant and so the baryon density at the edge of the lattice has to come from the main body of the configurations. In additions, simulations using different lattice shapes and sizes show that the baryon density accumulation is always as far away from the origin as possible; for example, in a square lattice with the origin placed off-centre the baryon density accumulation is to be found primarily in the farthest corner of the lattice, whereas for spherical lattices the accumulation is spread equally along the curved lattice edge.

One possibility is that, if the lattice size were extended to infinity, the configuration would radiate away all its spin energy in this manner. In investigating this, we first note that the spin energy does not seem to have any substantial effect on the main body of the configuration. Indeed, it is unclear whether it has any effect at all within the experimental error of the lattice simulations. Simulations on the $B = 1$ spin 3/2, isospin 3/2 configuration and on the $B = 2$ spin 1, isospin 0 configuration showed that the peak variance in the fields was less than .1% with the spin energy included. The peak variance is an order of magnitude larger than the peak ejected field value. However, the inertia increase, and hence the change in rotational energy, is almost entirely due to the ejected fields. It is fair to say that most, if not all, of the spin energy goes into radiating matter away from the configuration.

This is a very strong indication that, in fact, the configuration radiates away all its spin energy. One can also find evidence to support this hypothesis by seeing how the moments of inertia vary as the lattice sizes are increased. Again, our tests are run using the $B = 1$ spin 3/2, isospin 3/2 and $B = 2$ spin 1, isospin 0 configurations. In the $B = 1$ case, the simulations are done under the assumption of axial symmetry; all indications are that the spin energy radiates radially so the imposition of axial symmetry should have no change on the end state. We derive the energy of the axially symmetric $B = 1$ spin 3/2, isospin 3/2 configuration in section 4.3; a general

description of the terms are adequate here:

$$E_\Delta \sim \alpha\left(\frac{2}{V_2}+\frac{1}{V_3}\right)+\beta\frac{\left(1+\frac{W_2}{V_2}\right)^2}{U_2-\frac{W_2^2}{V_2}} \tag{4.1}$$

The energy is divided into isospin-only terms and spin-isospin cross terms whose magnitude depends on the divergence between spin and isospin. One can just as easily write the energy as the sum of spin terms and similar cross terms. Therefore, for the $B = 1$ configuration to radiate away all its spin matter, the value of the spin moments of inertia should tend towards those of the isospin moments of inertia as the lattice is made infinitely large; from the graph in figure 4-7, we see that in fact the spin inertia values tend quite quickly towards the isospin inertia values.

In contrast, the $B = 2$ configuration has spin energy only; the rotational energy is of the form

$$E \sim \alpha\left(\frac{1}{U_{ij}}\right) \tag{4.2}$$

and so the spin energy will be radiated away if the diagonal values of U_{ij} go to infinity as the lattice is made infinite. Indeed, our plot in figure 4-8 shows the diagonal values increasing as the lattice size increases.

Our investigations are curtailed by the size of the lattice and are by no means conclusive. However, the results obtained so far still are a very strong indication that the configuration radiates all its spin energy.

4.3 Modelling the nucleon and delta resonance

Our aim in the $B = 1$ simulations is to obtain the definitive zero-mode quantized Skyrme configurations corresponding to the nucleon and delta resonance, and thus complete the task begun by the rigid-body quantization in [8]. The parameters F_π and e obtained by fitting the configuration energies to the nucleon and delta masses for a given value of m_π can thus be settled, at least for the rotational case.

We initially annealed the two particles on a 70^3 lattice with spacing .12, using the same initial configurations. The inertial energy terms for the $l = k = 1/2$ nucleon

and $l = k = 3/2$ delta resonance, was obtained by finding the lowest eigenvalue of a 4×4 and 16×16 matrix respectively. Previous work [50] indicates that the nucleon in the Skyrme model is stable against quadrupole deformations and that nucleon deformations, to leading order, take place within a spherically symmetric ansatz. Our 3D results results indeed seem to bear this out, with $U_{ii} = V_{ii} = W_{ii}$ for all values of i to within lattice error. The $l = k = 3/2$ configuration showed signs of ejected energy for all values of pion mass.

We were mainly concerned with checking that the configurations had at least axial symmetry, so we could use the cartoon method described in section 3.4 to get much more accurate results. As well as axial symmetry, there is also a reflection symmetry in the xy-plane and so the principal axes of inertia can be taken as the standard orthogonal axes, with $U_{ij} = V_{ij} = W_{ij} = 0$ where $i \neq j$; we can set $U_{ii} = U_i$ and so forth.

We simplify the inertia matrix $\mathcal{U}$ using the axially-symmetric identities:

$$U_1 = U_2, \quad V_1 = V_2, \quad W_1 = W_2, \tag{4.3}$$

in which case $\mathcal{U}$ becomes:

$$\mathcal{U} = \begin{pmatrix} U_2 & 0 & 0 & -W_2 & 0 & 0 \\ 0 & U_2 & 0 & 0 & -W_2 & 0 \\ 0 & 0 & U_3 & 0 & 0 & -W_3 \\ -W_2 & 0 & 0 & V_2 & 0 & 0 \\ 0 & -W_2 & 0 & 0 & V_2 & 0 \\ 0 & 0 & -W_3 & 0 & 0 & V_3 \end{pmatrix} \tag{4.4}$$

We first consider the case of the nucleon; inverting $\mathcal{U}$ and putting the result into the matrix Hamiltonian (2.55) for the $l = k = 1/2$ representation of the direct product

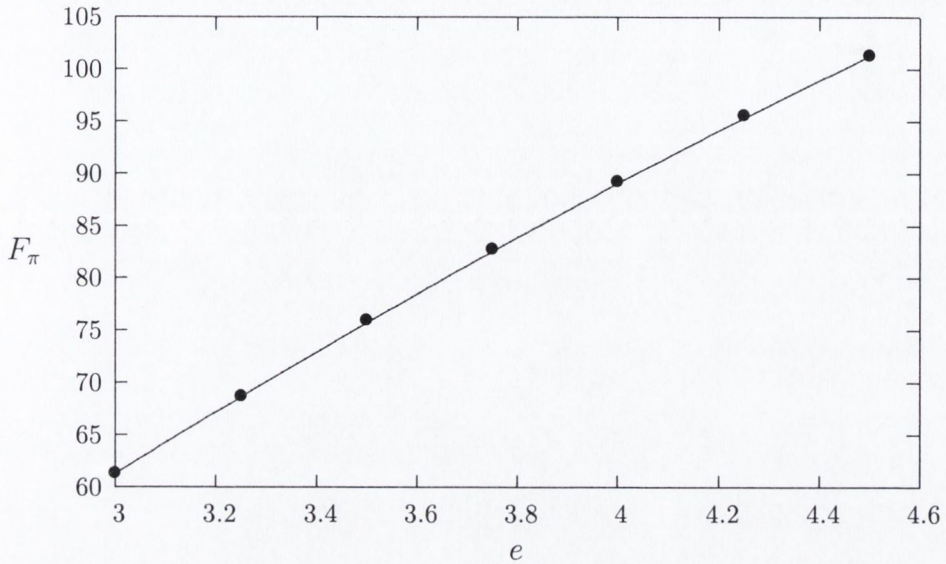

Figure 4-9: Plot of F_π, as a function of e, for which the energy $M + E_N$ is equal to the nucleon mass 939 MeV; the pion mass parameter m_π set to its experimental value of 138 MeV. Our results (bold circles) are compared with those obtained using the rigid body approach taken in [18] (solid line).

space of **L** and **K** gives:

$$H = \frac{\hbar}{4} \begin{pmatrix} \kappa_1 + \kappa_3 & 0 & 0 & 0 \\ 0 & \kappa_1 - \kappa_3 & \kappa_2 & 0 \\ 0 & \kappa_2 & \kappa_1 - \kappa_3 & 0 \\ 0 & 0 & 0 & \kappa_1 + \kappa_3 \end{pmatrix} \tag{4.5}$$

$$\begin{aligned} \kappa_1 &= \frac{1 + \frac{W_2}{V_2}^2}{U_2 - \frac{W_2^2}{V_2}} + \frac{1}{V_2} + \frac{\left(1 + \frac{W_3}{V_3}^2\right)}{2\left(U_3 - \frac{W_3^2}{V_3}\right)} + \frac{1}{2V_3} \\ \kappa_2 &= \frac{2\frac{W_2}{V_2}}{U_2 - \frac{W_2^2}{V_2}} \\ \kappa_3 &= \frac{\frac{W_3}{V_3}}{U_3 - \frac{W_3^2}{V_3}} \end{aligned} \tag{4.6}$$

Following [9], we simplify the Hamiltonian further by establishing a relation between U_3, V_3 and W_3 for axially symmetric fields. We first express the quantity

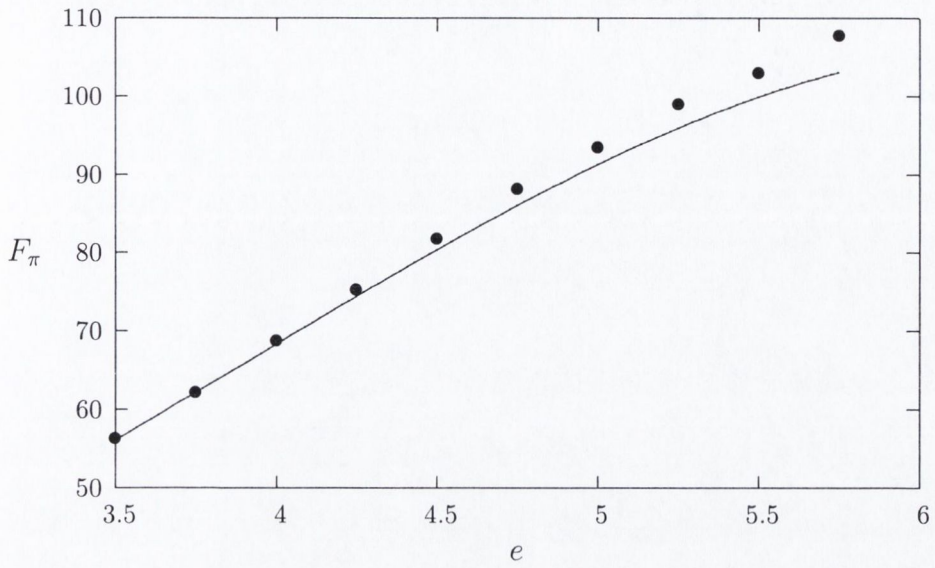

Figure 4-10: As Fig. 4-9, but with the pion mass parameter m_π set to the value of 345 MeV suggested in [29]. Our results (bold circles) are compared with those obtained using the rigid body approach taken in [18] (solid line).

$\epsilon_{3jk} x_j R_k$ in polar coordinates:

$$\begin{aligned} \epsilon_{3jk} x_j R_k &= (\mathbf{x} \times \nabla)_3 U U^\dagger \\ &= \frac{\partial U}{\partial \phi} U^\dagger . \end{aligned} \tag{4.7}$$

We can then identify $\epsilon_{ij3} x_j R_i$ and $-\frac{i}{2}[\sigma_3, U] U^\dagger$ by looking at the general form of an axially symmetric field with unit baryon number:

$$U = \mathrm{e}^{\frac{-i\sigma_3\phi}{2}} \mathrm{e}^{if(r,z) n_i \sigma_i} \mathrm{e}^{\frac{i\sigma_3\phi}{2}} \tag{4.8}$$

and taking its derivative with respect to ϕ:

$$\begin{aligned} \frac{\partial U}{\partial \phi} &= -\frac{i\sigma_3}{2} \left(\mathrm{e}^{-\frac{i\sigma_3\phi}{2}} \mathrm{e}^{if(r,z)} \mathrm{e}^{\frac{i\sigma_3\phi}{2}} \right) + \left(\mathrm{e}^{\frac{-i\sigma_3\phi}{2}} \mathrm{e}^{if(r,z)} \mathrm{e}^{\frac{i\sigma_3\phi}{2}} \right) \frac{i\sigma_3}{2} \\ &= -\frac{i}{2} [\sigma_3, U] . \end{aligned} \tag{4.9}$$

We see the expressions for the inertias U_3, V_3 and W_3 in the moment of inertia integrals

(2.51) differ only in the terms $\epsilon_{3jk}x_jR_k$ and $-\frac{i}{2}[\sigma_3, U]U^\dagger$, and so

$$U_3 = V_3 = W_3. \tag{4.10}$$

We did not insert this identity into the full Hamiltonian (2.55) initially because it would have made the matrix (4.4) singular. The elements of the matrix Hamiltonian (4.5) are modified by the relation:

$$\begin{aligned} \kappa_1 &= \frac{1 + \frac{W_2}{V_2}^2}{U_2 - \frac{W_2^2}{V_2}} + \frac{1}{V_2} + \frac{1}{2V_3}, \\ \kappa_2 &= \frac{2\frac{W_2}{V_2}}{U_2 - \frac{W_2^2}{V_2}}, \\ \kappa_3 &= 0. \end{aligned} \tag{4.11}$$

We can use a filter to ensure we only get eigenvalues of states corresponding to $L_3 = -K_3$. Using as columns the basis vectors of the null space of $K_3 + L_3$ in their right place we construct the matrix P

$$P = \begin{pmatrix} 0 & 0 & 0 & 0 \\ 0 & 1 & 0 & 0 \\ 0 & 0 & 1 & 0 \\ 0 & 0 & 0 & 0 \end{pmatrix} \tag{4.12}$$

The eigenvalues of PHP will correspond to states with $L_3 = -K_3$. There are two eigenvectors of H which are also eigenvectors of $L_3 + K_3$ with eigenvalue zero:

$$|0,0\rangle \equiv \frac{1}{\sqrt{2}}\left(|\frac{1}{2},-\frac{1}{2}\rangle \otimes |\frac{1}{2},\frac{1}{2}\rangle - |\frac{1}{2},\frac{1}{2}\rangle \otimes |\frac{1}{2},-\frac{1}{2}\rangle\right), \quad E_{0,0} = \frac{\hbar}{4}(\kappa_1 - \kappa_2) \tag{4.13}$$

and

$$|1,0\rangle \equiv \frac{1}{\sqrt{2}}\left(|\frac{1}{2},-\frac{1}{2}\rangle \otimes |\frac{1}{2},\frac{1}{2}\rangle + |\frac{1}{2},\frac{1}{2}\rangle \otimes |\frac{1}{2},-\frac{1}{2}\rangle\right), \quad E_{1,0} = \frac{\hbar}{4}(\kappa_1 + \kappa_2) \tag{4.14}$$

The first eigenvector is a spherically symmetric state and also has the lower energy

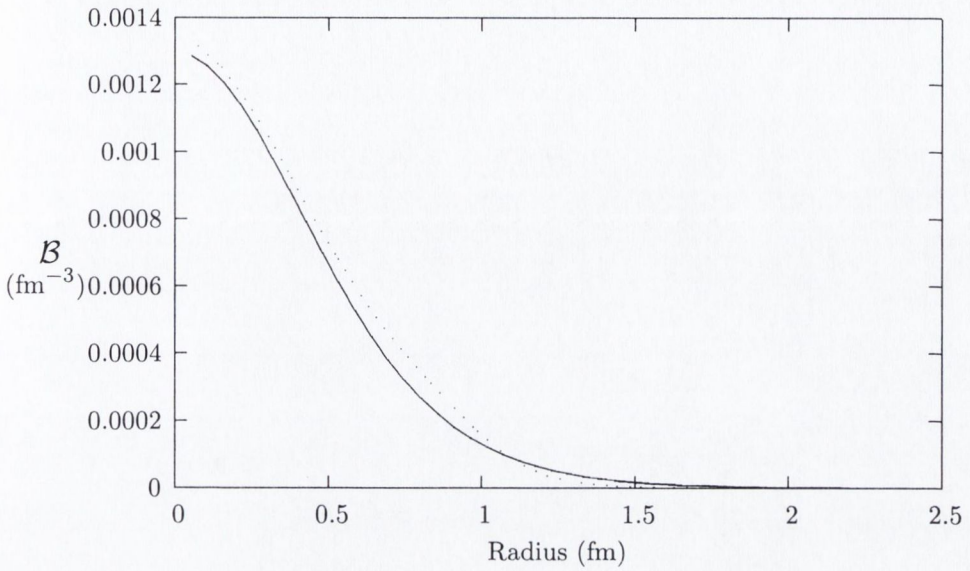

Figure 4-11: Plot of radial distribution of baryon density $\mathcal{B}$ for a spin 3/2, isospin 3/2 B=1 Skyrme configuration with m_π=345MeV (solid line), compared with distribution of an $m = 0$ classical Skyrmion (dotted line).

since κ_1 and κ_2 are always positive; hence

$$E_N = \frac{\hbar}{4}\left[\frac{\left(1-\frac{W_2}{U_2}\right)^2}{V_2-\frac{W_2^2}{U_2}}+\frac{1}{U_2}+\frac{1}{2U_3}\right] \tag{4.15}$$

and is therefore the energy of an axially symmetric nucleon. We see that in the spherically symmetric case $U_2 = U_3 = W_2 = V_2$, and E_N reduces to the rotational energy formula obtained in [8]:

$$E_N^{sym} = \frac{3}{4}\frac{\hbar}{2\Lambda} \tag{4.16}$$

where $\Lambda = \frac{1}{3}(U_1 + U_2 + U_3) = U_3$. The energies of all other eigenstates go to infinity in the spherically symmetric limit.

We find the energy of the spin 3/2, isospin 3/2 delta resonance in an identical manner to the nucleon, constructing direct product eigenstates of $\mathbf{L} \otimes \mathbf{K}$ using the 3/2 matrix representation of SU(2) and finding the lowest eigenstate of the resulting

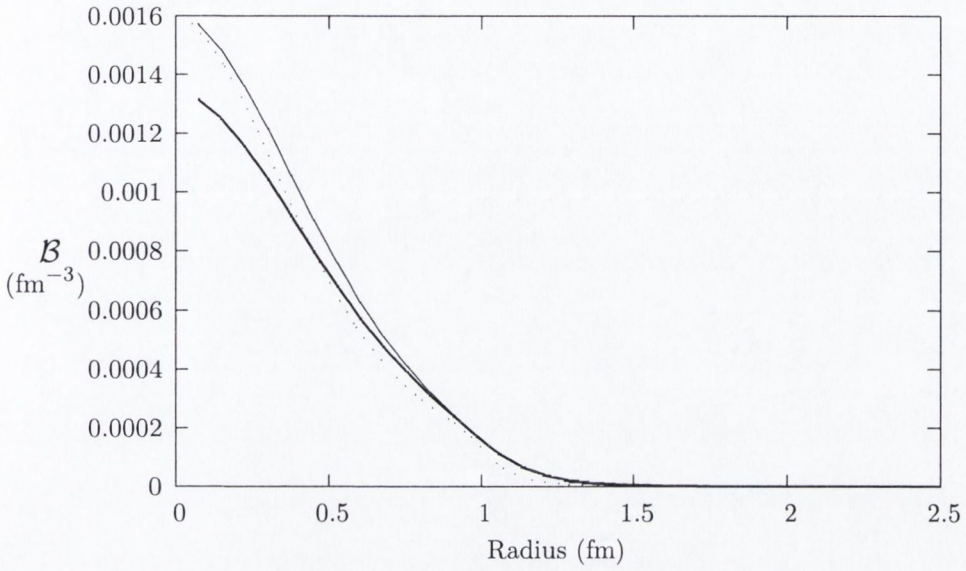

Figure 4-12: Plot of radial distribution of baryon density $\mathcal{B}$ for two different approaches towards quantizing a spin 3/2, isospin 3/2 B=1 Skyrme configuration with m_π=345MeV. The result of quantizing the lowest eigenvalue of a matrix Hamiltonian is shown by a solid line; the cross-section was taken at $\theta = \pi/2$, but other cross-sections taken at $\pi/8, \pi/4$, and $3\pi/8$ overlay exactly onto this line. The approach in [29] of quantizing the degree of freedom given by the cylindrical map ansatz (3.14) is shown with cross-sections at $\pi/4$ (thin line) and $\pi/2$ (dotted line).

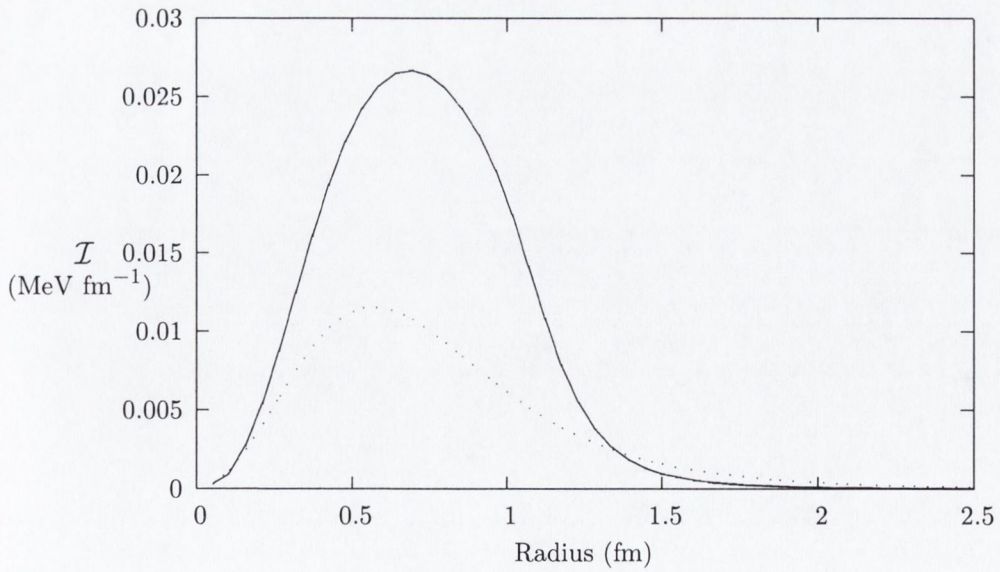

Figure 4-13: Plot of distribution of moment of inertia density $\mathcal{I}$ normal to the cylindrical axis of rotation for a spin 3/2, isospin 3/2 B=1 Skyrme with m_π=345MeV (solid line), compared with distribution of an $m = 0$ classical Skyrmion (dotted line).

Hamiltonian that is also a null eigenstate of $L_3 + K_3$:

$$|E_\Delta >= \frac{1}{\sqrt{2\,(1+\chi^2)}}\left[(1-\chi)\,|0,0> -(1+\chi)\,|2,0>\right] \tag{4.17}$$

where

$$\begin{aligned}
\chi &= \frac{U_2}{3W_2}\left(1-\frac{W_2}{U_2}\right)^2 + \left(\frac{U_2V_2-W_2^2}{3W_2}\right)\left(\frac{1}{U_2}-\frac{1}{U_3}-\sqrt{C}\right) \\
C &= \left[\frac{3\frac{W_2}{U_2}}{V_2-\frac{W_2^2}{U_2}}\right]^2 + \left[\frac{\left(1-\frac{W_2}{U_2}\right)^2}{V_2-\frac{W_2^2}{U_2}} - \left(\frac{1}{U_2}-\frac{1}{U_3}\right)\right]^2
\end{aligned} \tag{4.18}$$

$|E_\Delta\rangle$ is the axially symmetric delta state; its energy is

$$E_\Delta = \frac{\hbar}{4}\left[\frac{5\left(1-\frac{W_2}{U_2}\right)^2+6\frac{W_2}{U_2}}{V_2-\frac{W_2^2}{U_2}} + \frac{5}{U_2} + \frac{5}{2U_3} - 2\sqrt{C}\right] \tag{4.19}$$

In the spherically symmetric case, χ goes to -1, $|E_\Delta\rangle$ is the singlet $|0,0\rangle$ state, and the energy (4.19) again reduces to the rotational energy formula obtained in [8]:

$$E_\Delta^{sym} = \frac{15}{4}\frac{\hbar}{2\Lambda} \tag{4.20}$$

with the energy of all other eigenstates going to infinity.

Our annealing was carried out on a quarter-disc lattice with a radius of 250 lattice points spaced a distance of .06 apart. This configuration gave rise to errors 0.5% arising from the lattice spacing and .2% arising from the finite lattice size. Our results were crosschecked with full 3D simulations and found to be identical within the lattice errors of the 3D simulation. For the $l = k = 1/2$ configuration all moments of inertia are equal; for the $l = k = 3/2$ the ejected energy causes a divergence of U_2 from the other moments of inertia V_2, V_3 and W_2; this divergence was around 2% for a lattice radius of 250 points spaced .06 apart.

Our approach can be compared with that of [29] which also annealed a $B = 1$ configuration on a 2D lattice using axial symmetry. Instead of quantizing the

fields as shown above and then using the cylindrical field ansatz (3.14) in the lattice implementation, they make the approximation of substituting the ansatz into the Lagrangian (2.12), resulting in the energy

$$E_{app} = \frac{\hbar}{2V_3} l\,(l+1) \tag{4.21}$$

One could say that this procedure is guided by classical intuition; classically the particle is expected to bulge in a direction normal to the rotation axis and so one might expect the normal degree of freedom is the one to quantize. However in quantization, there is no preferred axis of rotation and the order of magnitude of the rotational energy terms is the same in each direction.

In figure 4-9 and figure 4-10 the results of our nucleon simulations are shown in comparison with results obtained using the rigid body approximation used in [18]. The pion mass m_π was set to its experimental value of 138 MeV in figure 4-9, whereas in figure 4-10 it was set to the larger value of 345MeV suggested in [29]; we see that the variation from the rigid-body solution is not significant and indeed only becomes noticeable at the higher value of the pion mass. In this case our results do not differ substantially from those in [29], the main reason being that the deformation from the rigid-sphere quantization result is very small in both cases.

The deformation from the classical minimum in the $l = k = 3/2$ case is much larger than in the $l = k = 1/2$ case, large enough to cause a noticeable bulge in the configuration for the approach in [29]. However with our approach, and leaving the ejected energy aside, every indication points to the configuration having spherical symmetry. Baryon density cross-sections taken at different angles to the symmetry axis are as close to each other as to be indistinguishable, as are those of U_2, V_2 and W_2 away from the lattice edge at any given angle to the symmetry axis.

The approach in [29] does not have any ejected energy as the U_3 is constrained by the symmetry to be equal to V_3. The minimum energy configuration has a lower energy than our approach, in line with the predictions of [51] using restricted oblate modifications of Skyrme hedgehog configurations. However this is a result of the lack of rigour in the quantization.

One final question; why does the $l = k = 3/2$ eject energy whilst the $l = k = 1/2$ B=1 Skyrmion does not? The short answer is that the Skyrmion does not spin fast enough to produce any rotational effects; there is no significant deviation from our result and that using the rigid-sphere approach in [18]. One might argue that the higher charge configurations spin much more slowly and yet still eject matter. However, the nucleon is spherically symmetric, and so spin and isospin are constrained to be equal. In the nucleon case, the spin energy is not high enough for the spin and isospin degrees of freedom to separate. One might suspect that for higher pion masses, the increased spin energy due to the lower moments of inertia might cause the configuration to radiate matter; preliminary results suggest that this might indeed be the case.

4.4 Higher charge rotating configurations

As we discussed in section 2.4.2, we wish to investigate the the possibility that the Skyrme configuration that is a minimum in the zero mode configuration space might deviate sufficiently from the classical minimum energy to give ground state quantum numbers consistent with experiment. The quantization is carried out without symmetry impositions so that the annealed configuration changes the entire space of rotational and isorotational deformations.

Our quantum treatment of the nucleon and delta resonance in section 4.3 yielded rotational energy terms which averaged rotations over all directions, and maintained the spherical symmetry. In effect, there is no preferred axis of rotation, and instead of a rotational bulge we get a radial expansion in all directions. For $B > 1$ the rotational energy contribution drops due to increasing inertias, and so we expect rotational effects to be less marked for higher values of B.

Due to lattice size constraints, we cannot anneal configurations of $B > 5$ without a significantly large pion mass. The pion mass does have the effect of lowering the inertias and increasing the rotational energy contribution; however, even with the pion mass the zero mode energy does not have a significant effect on the configuration. The $B = 7$ configuration, for example, does not differ significantly from the annealed

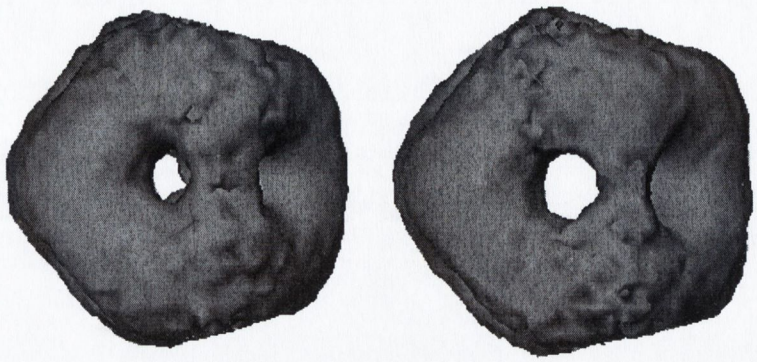

Figure 4-14: Baryondensity surface of two spin 3/2 isospin 1/2 $B = 5$ configurations at $m = 0$, for values of $e = 8.6$ and $e = 12.2$; this corresponds to values of $\hbar$ of 150 and 300 respectively.

solution in figure 4-3.

The pion mass energy term is a central potential; from our $B = 1$ simulations it appears the rotational energy term is also. It is therefore reasonable to investigate whether a configuration with a very large rotational energy will change shape in expanding in the same way that a configuration with large pion mass changes shape in contracting. The rotational energy is proportional to $\hbar^2$, which is in turn equal to $4e^4$; there may be a critical value of the free parameter e above which the shape is changed from the classical minimum.

The $B = 5$ configuration is the configuration with the lowest baryon number for which the polyhedral skeleton has unequal polygonal faces; we recall that shape change with the addition of the pion mass only took place in when the polyhedral skeletons were non-Platonic. Our simulations took place with $m_\pi = 0$ and different values of e up to two and a half times that of the value used in our $B = 1$ simulations. Isodensity surfaces for two values of e can be seen in figure 4-14; so far, no conclusive evidence of shape change has been seen, and indeed the zero mode energy appears not to have any significant effect on the configuration. However, for $B = 5$, rotational energies only begin to equal large pion mass energies at for values of e at five times that used in our $B = 1$ simulations, and investigations are continuing in this parameter range.

Chapter 5

Conclusion

The simulated annealing technique has enabled us to shed considerable light on the static configurations of the Skyrme model, yielding three primary findings of importance.

1. A quantized treatment of the Skyrme model does not pick out a preferred axis of rotation, and as a result the rotational energy of the quantized configuration is an average of contributions from all rotational axes. The $B = 1$ Skyrme minimum energy configurations therefore remain spherically symmetric with the addition of rotational energy. Configurations with $B > 1$ are not affected considerably by rotational energy due to their high moments of inertia.

2. Allowing the spatial spin degrees of freedom to influence the configuration causes a small ejection of matter towards the edge of the lattice while leaving the configuration practically unchanged. We have found evidence to suggest that the configuration radiates away all its spatial rotation energy.

3. For large pion masses, non-Platonic configurations change in shape compared to their equivalents without pion mass; Platonic configurations are changed in size only. The shape change for non-Platonic configurations is such that the rational map is no longer a good approximation.

It is our discovery that Skyrme configurations radiate away their spin energy that has the most immediate consequences for the future of the Skyrme model. If it is

true, then it would spell the end of the Skyrme model as a useful theory of nuclear physics, as there is no way of distinguishing states of different spin in the model. The evidence to suggest that all the spin energy is radiated is convincing, but more needs to be done to conclusively show this, and also that the radiation is physical and not due to some unknown computational irregularity.

Both these issues can be addressed by obtaining the same results using a different numerical scheme, namely, evolving the full field equations in time. This method has already been in use for some time to generate minimum energy field configurations [7], and it has the advantage that we would be able to see the process of radiation in the course of the algorithm run, compared to SA where we can only see the final configuration. Evolving the full field equations is time-consuming, and a minimum enrgy configuration using the matrix Hamiltonian method method used here cannot yet be obtained within a reasonable time. However, it would suffice to show that the same effect happens using SA and full-field evolution using a simplified rotational energy term, for example

$$E = E_{cl} + \frac{\hbar^2}{U_2}, \tag{5.1}$$

the energy of a toroidal configuration like the $B = 2$ toroid describing the deuteron [9].

Even if the zero mode Skyrme configuration is stable, the addition of the zero modes will not provide the correct quantum numbers. At the beginning of our research, we believed the zero modes would cause the symmetry-breaking deformation and the pion mass would influence the radial deformation; it seems now that the reverse is the case. This does not necessarily mean that configurations with pion mass will yield the correct quantum numbers; the configurations we have generated so far do not differ in their point symmetry group to their zero pion mass equivalents. In addition, Platonic configurations such as $B = 7$, which have the most restrictions on allowed quantum numbers l and k, appear to differ from the $m_\pi = 0$ configuration in scale only.

It is known that the spectrum of rotational states is widened with the addition of higher mode degrees of freedom [15]; the general consensus, however, is that obtaining

minimum energy configurations with vibrational degrees of freedom added is much more difficult. At present, vibrational mode spectra are usually treated as small fluctuations around the classical minimum and, as such, the treatment relies on the symmetries of the classical minimum in order to classify them. One approach [30, 32] involves treating the vibrations as small harmonic perturbations around the static configuration $U_{static}(\mathbf{x})$

$$U(\mathbf{x}) = U_{static}(\mathbf{x}) + \sum_{modes} \epsilon_n \delta_n(\mathbf{x}) \cos(\omega_n t) + \mathrm{O}(\epsilon^2) \tag{5.2}$$

where the functions $\delta_n(\mathbf{x})$ obeying

$$\delta_n(\mathbf{x}) . U_n(\mathbf{x}) = 0 \tag{5.3}$$

are normal modes, each excited with frequency ω_n and amplitude ϵ_n.

The power spectrum was found by perturbing the classical minimum and using full field simulations to evolve the configuration in time; ω_n and ϵ_n were found by Fourier analysis of $U(\mathbf{x})$ at any lattice point. Once ω_n have been identified, the maps $\delta_n(\mathbf{x})$ can then be identified by performing another full field evolution and by Fourier analysing each component of $U(\mathbf{x})$.

Perhaps one idea might be to anneal with respect to the energy of this configuration

$$E = E_{cl} + E_{rot} + \hbar \sum_{n}^{modes} \omega_n \tag{5.4}$$

If the Skyrmion then deforms, new full field evolutions can then be run to determine the new ω_n, and another annealing run performed; the procedure continues until the configuration stabilises.

Bibliography

[1] E. Rutherford, Phil. Mag. **21** (1911) 669.

[2] G. 't Hooft, Nucl. Phys. **B75** (1974) 461.

[3] E. Witten, Nucl. Phys. **B160** (1979) 57.

[4] T. H. R. Skyrme, Proc. Roy. Soc. **A260** (1961) 127.

[5] I. Zahed and G.E. Brown, Phys. Reports **142** (1986) Nos 1 and 2.

[6] A. Jackson, A.D. Jackson and V. Pasquier, Nucl. Phys. **A432** (1985) 367.

[7] R.A. Battye and P.M. Sutcliffe, Phys. Rev. Lett. **79** (1997) 363, ⟨hep-th/0410157⟩.

[8] G.S. Adkins, C.R. Nappi and E. Witten, Nucl. Phys. **B228** (1983) 552.

[9] E. Braaten and L. Carson, Phys. Rev. **D38** (1988) 720.

[10] E. Braaten, S. Townsend and L. Carson, Phys. Rev. **D38** (1988) 720.

[11] R.A. Battye and P.M. Sutcliffe, Rev. Math. Phys. **14** (2002) 29.

[12] R. Rajaraman, H.M. Sommermann, J. Wambach and H.W. Wyld, Phys. Rev. **D33** (1986) 287.

[13] E. Braaten and J.P. Ralston, Phys. Rev. **D31** (1985) 598.

[14] S. Krusch, Annals Phys. **304** (2003) 103, ⟨hep-th/0210310⟩.

[15] P. Irwin, Phys. Rev **D61** (2000) 114021, ⟨hep-th/9804142⟩.

[16] R.A. Battye and P.M. Sutcliffe, Nucl. Phys. **B705** (2005) 384, ⟨hep-th/0410157⟩.

[17] G.H. Derrick, J. Math. Phys. **5** (1964) 1252.

[18] G.S. Adkins and C.R. Nappi, Nucl. Phys. **B233** (1984) 109.

[19] G.S. Adkins and C.R. Nappi, Phys. Lett. **B137** (1984) 251.

[20] I. Floratos and B. Piette, Phys. Rev. **D64** (2001) 0405009.

[21] J.-P. Longpre and L. Marleau, Phys. Rev. **D71** (2005) 3598, ⟨hep-th/0502253⟩.

[22] C. Nash and S. Sen, *Differential topology for physicists*, Academic Press (1983).

[23] N.S. Manton and P.M. Sutcliffe, *Topological solitons*, Cambridge University Press (2004).

[24] E. Witten, Nucl. Phys. **B223** (1983) 433.

[25] C.J. Houghton, N.S. Manton and P.M. Sutcliffe, Nucl. Phys. **B510** (1998) 507, ⟨hep-th/9705151⟩.

[26] S. Jarvis, *A rational map for Euclidean monopoles via radial scattering*, Oxford preprint (1996).

[27] Ch. Hadjuk and B. Schweisinger, Phys. Lett. **B140** (1984) 172.

[28] A. Hayashi and G. Holzwarth, Phys. Lett. **B140** (1984) 175.

[29] R.A. Battye, S. Krusch and P.M. Sutcliffe, *Spinning Skyrmions and the Skyrme parameters*, preprint (2005), ⟨hep-th/0507279⟩.

[30] C. Barnes, K. Baskerville and N. Turok, Phys. Rev. Lett. **79** (1997) 367, ⟨hep-th/9711071⟩.

[31] R.A. Leese, N.S. Manton and B.J. Schroers, Nucl. Phys. **B442** (1995) 228. ⟨hep-th/9502045⟩.

[32] N. Walet, Nucl. Phys. **A606** (1996) 429.

[33] C. Barnes and N. Turok, *A technique for calculating quantum corrections to solitons*, preprint (2005), ⟨hep-th/9711071⟩.

[34] D. Finkelstein and J. Rubenstein J. Math. Phys. **11** (1968) 1762.

[35] J. G. Williams, J. Math. Phys. **11** (1970) 2611.

[36] E. Braaten and L. Carson, Phys. Rev. Lett. 56 (1986) 567.

[37] S. Krusch, *Finkelstein-Rubinstein constraints for the Skyrme model with pion masses*, preprint (2005), ⟨hep-th/0509094⟩.

[38] S. Kirkpatrick, C.D. Gelatt and M.P. Vecchi, Science **220** (1983) 671.

[39] S. Geman and D. Geman, IEEE Transactions on Pattern Analysis and Machine Intelligence **6** (1984) 721.

[40] L. Ingber, Control and Cybernetics **25** (1996) 33.

[41] A. Corana, M. Marchesi, C. Martini and S. Ridella, (ACM) Transactions on Mathematical Software **13** (1987) 262.

[42] P. Siarry, G. Berthiau, F. Durdin and J. Haussy, (ACM) Transactions on Mathematical Software **23** (1997) 209.

[43] M. Hale, O. Schwindt and T. Weidig, Phys. Rev. **E62** (2001) 4333, ⟨hep-th/0002058⟩.

[44] P.M. Sutcliffe, Phys. Lett. **B292** (1992) 104.

[45] M. Peardon, private communication.

[46] M.F. Atiyah and N.S. Manton, Phys. Lett. **B222** (1989) 430.

[47] M. Alcubierre, S. Brandt, B. Brugmann, D. Holz, E. Seidel, R. Takahashi and J. Thornburg, Int. J. Mod. Phys. **D10** (2001) 273, ⟨gr-qc/9908012⟩.

[48] D.J. Wales and H.A. Scheraga, Science. **285** (1999) 1368.

[49] B.W. Wah and T. Wang, *Proc. Principles and Practices of Constraint Programming*, Springer-Verlag (1999) p461.

[50] Ch. Hadjuk and B. Schweisinger, Phys. Lett. **B145** (1984) 171.

[51] L. Marleau,*Deformed Skyrmions*, Talk given at 'A CRM-Fields-CAP Summer Workshop in Theoretical Physics: Solitons, Properties, Dynamics, Interactions and Applications, Kingston, Ontario, Canada, 20-26 Jul 1997, ⟨hep-th/9710369⟩.

[52] N. Dorey, M.P. Mattis and J. Hughes, Phys. Rev. **D49** (1994) 3598.

[53] R.A. Battye and P.M. Sutcliffe, Phys. Lett. **B391** (1997) 150.